6

Three-dimensional beam theory

In the previous chapter, Euler-Bernoulli theory is developed for beams under axial and transverse loads. The analysis is limited, however, to deformations of the beam in plane $(\bar{\imath}_1, \bar{\imath}_2)$. This behavior can be observed, for instance, when the cross-section of the beam presents a plane of symmetry and the only applied loads are acting in this plane.

In numerous practical applications, the beam's cross-section presents no particular symmetries and is instead of arbitrary shape. In addition, the applied loads may act along several distinct directions and not just in plane $(\bar{\imath}_1, \bar{\imath}_2)$. Consider an aircraft wing: the cross-section is of a complex shape involving curved skins and two or more spars, and the wing is subjected lift and drag forces. In the case of a helicopter blade, large centrifugal forces generated by the rotation of the blade are also present. Similarly, machine components often operate in a complex, three-dimensional loading environment.

Figure 6.1 shows a beam of arbitrary cross-sectional shape subjected to a complex three-dimensional loading. This loading consists of distributed and concentrated axial and transverse loads, as well as distributed and concentrated moments. The axial and transverse distributed loads, $p_1(x_1)$, $p_2(x_1)$, and $p_3(x_1)$ act along directions, $\bar{\imath}_1$, $\bar{\imath}_2$, and $\bar{\imath}_3$, respectively. The same convention is used for the concentrated loads $P_1^{[k]}$, $P_2^{[k]}$, and $P_3^{[k]}$, but in this case it is necessary to add a second index to identify the k^{th} concentrated load in the direction specified by the first index: $P_3^{[2]}$ is the second concentrated force acting along axis $\bar{\imath}_3$. Distributed moments, $q_2(x_1)$ and $q_3(x_1)$, acting about axes $\bar{\imath}_2$ and $\bar{\imath}_3$, respectively, can be introduced in a similar manner. Concentrated moments $Q_2^{[k]}$ and $Q_3^{[k]}$ act about the same axes.

Figure 6.1 depicts concentrated forces and moments acting at the tip of the beam, but in practical situations, such concentrated loads could be applied at any spanwise location. The notation used in this text for the various loads is summarized in table 6.1. The subscript indicates the direction of the loading component. If multiple concentrated loads are applied, a second subscript might be used to keep track of individual concentrated loads.

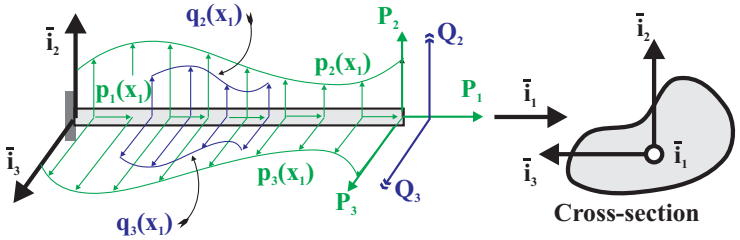

Fig. 6.1. Beam with arbitrary three-dimensional loading.

Table 6.1. Loading components acting on the beam.

Loading Type	Notation	Units
Distributed loads	$p_1(x_1), p_2(x_1), p_3(x_1)$	N/m
Concentrated loads	$P_1^{[k]}, P_2^{[k]}, P_3^{[k]}$	N
Distributed moments	$q_2(x_1), q_3(x_1)$	N.m/m
Concentrated moments	$Q_2^{[k]}, Q_3^{[k]}$	N.m

This three-dimensional loading is general, with an important exception: no torsional loads are applied, and the transverse loads are assumed to be applied in such a manner that the beam will bend without twisting. This important restriction will be removed in a later chapter after the study of the torsional behavior of beams. As mentioned earlier, the cross-section of the beam is of arbitrary shape. The origin of the axes has not yet been specified, and the orientation of axes $\bar{i}_2$ and $\bar{i}_3$ within the plane of the section is arbitrary, as depicted in fig. 6.1.

6.1 Kinematic description

The development of the three-dimensional beam theory starts with the three Euler-Bernoulli assumptions discussed in section 5.1. These assumptions are of a purely kinematic nature and are shown to imply the following displacements field

$$u_1(x_1, x_2, x_3) = \bar{u}_1(x_1) + x_3 \Phi_2(x_1) - x_2 \Phi_3(x_1), \tag{6.1a}$$
$$u_2(x_1, x_2, x_3) = \bar{u}_2(x_1), \tag{6.1b}$$
$$u_3(x_1, x_2, x_3) = \bar{u}_3(x_1). \tag{6.1c}$$

where the origin of the axis system on the cross-section is not yet specified. The corresponding strain field is shown to be

$$\varepsilon_2 = 0; \quad \varepsilon_3 = 0; \quad \gamma_{23} = 0, \tag{6.2a}$$
$$\gamma_{12} = 0; \quad \gamma_{13} = 0, \tag{6.2b}$$
$$\varepsilon_1(x_1, x_2, x_3) = \bar{\varepsilon}_1(x_1) + x_3\, \kappa_2(x_1) - x_2\, \kappa_3(x_1). \tag{6.2c}$$

6.2 Sectional constitutive law

Assume now that the beam is made of linearly elastic, isotropic material for which the stress-strain relationships are adequately described by Hooke's law, eq. (5.14). Because the cross-section does not deform in its own plane, the stress components, σ_2 and σ_3, acting in the plane of the section are far smaller than the axial stress component, σ_1, and Hooke's law is shown to reduce to eq. (5.14). The axial stress distribution is found by introducing eq. (6.2c) into eq. (5.14) to find

$$\sigma_1(x_1, x_2, x_3) = E\left[\bar{\varepsilon}_1(x_1) + x_3\,\kappa_2(x_1) - x_2\,\kappa_3(x_1)\right] \tag{6.3}$$

The axial force, N_1, is now evaluated by introducing this axial stress distribution into eq. (5.8) to find

$$\begin{aligned} N_1(x_1) &= \int_{\mathcal{A}} \sigma_1 \,\mathrm{d}\mathcal{A} = \int_{\mathcal{A}} E\bar{\epsilon}_1 \,\mathrm{d}\mathcal{A} + \int_{\mathcal{A}} Ex_3\kappa_2 \,\mathrm{d}\mathcal{A} - \int_{\mathcal{A}} Ex_2\kappa_3 \,\mathrm{d}\mathcal{A} \\ &= \left[\int_{\mathcal{A}} E \,\mathrm{d}\mathcal{A}\right] \bar{\epsilon}_1 + \left[\int_{\mathcal{A}} Ex_3 \,\mathrm{d}\mathcal{A}\right] \kappa_2 - \left[\int_{\mathcal{A}} Ex_2 \,\mathrm{d}\mathcal{A}\right] \kappa_3 \\ &= S\,\bar{\epsilon}_1(x_1) + S_3\,\kappa_2(x_1) - S_2\,\kappa_3(x_1), \end{aligned} \tag{6.4}$$

where the following sectional stiffness coefficients are defined

$$S = \int_{\mathcal{A}} E \,\mathrm{d}\mathcal{A}; \quad S_2 = \int_{\mathcal{A}} Ex_2 \,\mathrm{d}\mathcal{A}; \quad S_3 = \int_{\mathcal{A}} Ex_3 \,\mathrm{d}\mathcal{A}. \tag{6.5}$$

The bending moments, M_2 and M_3, acting about axes $\bar{\imath}_2$ and $\bar{\imath}_3$, respectively, are evaluated by introducing the axial stress distribution eq. (6.3) into eq. (5.11) to find

$$\begin{aligned} M_2 &= \int_{\mathcal{A}} x_3\sigma_1 \,\mathrm{d}\mathcal{A} = \int_{\mathcal{A}} x_3 E\bar{\epsilon}_1 \,\mathrm{d}\mathcal{A} + \int_{\mathcal{A}} Ex_3^2\kappa_2 \,\mathrm{d}\mathcal{A} - \int_{\mathcal{A}} Ex_2x_3\kappa_3 \,\mathrm{d}\mathcal{A} \\ &= \left[\int_{\mathcal{A}} Ex_3 \,\mathrm{d}\mathcal{A}\right] \bar{\epsilon}_1 + \left[\int_{\mathcal{A}} Ex_3^2 \,\mathrm{d}\mathcal{A}\right] \kappa_2 - \left[\int_{\mathcal{A}} Ex_2x_3 \,\mathrm{d}\mathcal{A}\right] \kappa_3 \\ &= S_3\,\bar{\epsilon}_1(x_1) + H_{22}\,\kappa_2(x_1) - H_{23}\,\kappa_3(x_1), \end{aligned} \tag{6.6}$$

and

$$\begin{aligned} M_3 &= -\int_{\mathcal{A}} x_2\sigma_1 \,\mathrm{d}\mathcal{A} = -\int_{\mathcal{A}} x_2 E\bar{\epsilon}_1 \,\mathrm{d}\mathcal{A} - \int_{\mathcal{A}} x_2 Ex_3\kappa_2 \,\mathrm{d}\mathcal{A} + \int_{\mathcal{A}} Ex_2^2\kappa_3 \,\mathrm{d}\mathcal{A} \\ &= -\left[\int_{\mathcal{A}} Ex_2 \,\mathrm{d}\mathcal{A}\right] \bar{\epsilon}_1 - \left[\int_{\mathcal{A}} Ex_2x_3 \,\mathrm{d}\mathcal{A}\right] \kappa_2 + \left[\int_{\mathcal{A}} Ex_2^2 \,\mathrm{d}\mathcal{A}\right] \kappa_3 \\ &= -S_2\,\bar{\epsilon}_1(x_1) - H_{23}\,\kappa_2(x_1) + H_{33}\,\kappa_3(x_1), \end{aligned} \tag{6.7}$$

where the following additional sectional stiffness coefficients are defined

$$H_{22} = \int_{\mathcal{A}} E\,x_3^2 \,\mathrm{d}\mathcal{A}; \quad H_{33} = \int_{\mathcal{A}} E\,x_2^2 \,\mathrm{d}\mathcal{A}; \tag{6.8}$$

$$H_{23} = \int_{\mathcal{A}} E\, x_2 x_3 \, \mathrm{d}\mathcal{A}. \tag{6.9}$$

The axial stiffness, S, is found in section 5.4 to characterize the axial stiffness of the beam and in section 5.5 the bending stiffness, H_{33}, is found to characterize the bending behavior of the beam about axis $\bar{\imath}_3$. The bending stiffness H_{22} plays the same role, but for bending about axis $\bar{\imath}_2$. A new bending stiffness coefficient, H_{23}, is called the *cross bending stiffness*.

Equations (6.4), (6.6) and (6.7) can be rewritten in a more compact matrix form as follows

$$\begin{Bmatrix} N_1(x_1) \\ M_2(x_1) \\ M_3(x_1) \end{Bmatrix} = \begin{bmatrix} S & S_3 & -S_2 \\ S_3 & H_{22} & -H_{23} \\ -S_2 & -H_{23} & H_{33} \end{bmatrix} \begin{Bmatrix} \bar{\epsilon}_1(x_1) \\ \kappa_2(x_1) \\ \kappa_3(x_1) \end{Bmatrix}. \tag{6.10}$$

These equations express a general linear relationship between the sectional stress resultants and the sectional strains. Thus, they are the constitutive laws for the cross-section of the beam, and the matrix on the right hand side of eq. (6.10) is called the *sectional stiffness matrix*. Clearly, these equations are fully coupled: all of the sectional strains affect the values of each of the sectional stress resultants. For example, the axial force $N_1(x_1)$ is not proportional only to the axial strain $\bar{\epsilon}_1(x_1)$, nor are the bending moments proportional only to curvatures. Instead, the behavior is fully coupled through the sectional coupling stiffness coefficients S_2, S_3 and H_{23} that appear in the off-diagonal entries of the sectional stiffness matrix. This means that an axial force, N_1, will appear as a result of an axial strain, $\bar{\epsilon}_1$, but also in the presence of curvatures, κ_2 or κ_3. Similarly, a bending moment appears as a result of either the κ_2 or κ_3 curvatures, but also in the presence of an axial strain, $\bar{\epsilon}_1$.

A general formulation of three dimensional Euler-Bernoulli beam theory can be developed based on the constitutive laws of eq. (6.10). Unfortunately, this leads to complex governing differential equations for the problem and this approach will not be pursued further. Rather, it will be shown that the sectional constitutive laws can be simplified by selecting the axis system appropriately. Indeed, in the formulation developed thus far, the origin of the axis system is arbitrary, and although the orientation of axis $\bar{\imath}_1$ is along the axis of the beam, the orientations of axes $\bar{\imath}_2$ and $\bar{\imath}_3$ within the plane of the cross-section are also arbitrary.

More specifically, the *origin of the axis system can be selected to coincide with the centroid of the section*, *i.e.*,

$$x_{2c} = \frac{1}{S}\int_{\mathcal{A}} E\, x_2 \, \mathrm{d}\mathcal{A} = \frac{S_2}{S} = 0; \quad x_{3c} = \frac{1}{S}\int_{\mathcal{A}} E\, x_3 \, \mathrm{d}\mathcal{A} = \frac{S_3}{S} = 0, \tag{6.11}$$

where the sectional coefficients, S_2 and S_3, are defined in eq. (6.5). The sectional constitutive laws, eq. (6.10), reduces to a partially uncoupled form

$$\begin{Bmatrix} N_1(x_1) \\ M_2(x_1) \\ M_3(x_1) \end{Bmatrix} = \begin{bmatrix} S & 0 & 0 \\ 0 & H_{22}^c & -H_{23}^c \\ 0 & -H_{23}^c & H_{33}^c \end{bmatrix} \begin{Bmatrix} \bar{\epsilon}_1(x_1) \\ \kappa_2(x_1) \\ \kappa_3(x_1) \end{Bmatrix}. \tag{6.12}$$

The bending stiffness coefficient, H_{22}, H_{33}, and H_{23}, are now replaced by their counterparts, H^c_{22}, H^c_{33}, and H^c_{23}, evaluated with respect to the centroid of the cross-section.

It is important to note that these partially uncoupled equations show that the axial force N_1 is now related to only the axial strain $\bar{\epsilon}_1$ and that the bending moments are related to the curvatures κ_2 and κ_3 only. This decoupling of the axial and bending behavior results from **locating the origin of the axis system the centroid of the cross-section**, rather than at an arbitrary point of the section. The two bending moments and corresponding curvatures, however, are still coupled due to the presence of the stiffness coefficient, H^c_{23}.

For most problems, the forces and moments are specified and it is required to find the resulting displacements and internal stresses. The sectional constitutive equations, eqs. (6.12), must therefore be inverted and solved for the sectional strain, $\bar{\epsilon}_1$, and curvatures, κ_2 and κ_3, in terms of stress resultants, N_1, M_2 and M_3. This results in

$$\begin{Bmatrix} \bar{\epsilon}_1(x_1) \\ \kappa_2(x_1) \\ \kappa_3(x_1) \end{Bmatrix} = \begin{bmatrix} 1/S & 0 & 0 \\ 0 & H^c_{33}/\Delta_H & H^c_{23}/\Delta_H \\ 0 & H^c_{23}/\Delta_H & H^c_{22}/\Delta_H \end{bmatrix} \begin{Bmatrix} N_1(x_1) \\ M_2(x_1) \\ M_3(x_1) \end{Bmatrix}, \tag{6.13}$$

where $\Delta_H = H^c_{22}H^c_{33} - H^c_{23}H^c_{23}$.

The axial stress can now be found by substituting these results into eq. (6.3) to find

$$\sigma_1 = E\left[\frac{N_1}{S} + x_3\,\frac{H^c_{33}M_2 + H^c_{23}M_3}{\Delta_H} - x_2\,\frac{H^c_{23}M_2 + H^c_{22}M_3}{\Delta_H}\right], \tag{6.14}$$

or, with minor rearrangements,

$$\sigma_1 = E\left[\frac{N_1}{S} - \frac{x_2H^c_{23} - x_3H^c_{33}}{\Delta_H}\,M_2 - \frac{x_2H^c_{22} - x_3H^c_{23}}{\Delta_H}\,M_3\right]. \tag{6.15}$$

This is a key result because it relates the axial stress distribution to the stress resultants which are, in turn, functions of the applied loads.

6.3 Sectional equilibrium equations

To complete the theory, equilibrium equations must also be derived. Consider an infinitesimal slice of the beam of length $\mathrm{d}x_1$ as depicted in fig. 6.2. The axial force, N_1, acts on the face at span-wise location x_1. A Taylor's series expansion is then used to express this axial force at location $x_1 + \mathrm{d}x_1$. Higher order differential terms are neglected, leading to the contribution shown in fig. 6.2. Summing all the forces in the axial direction yields the axial equilibrium equation

$$\frac{\mathrm{d}N_1}{\mathrm{d}x_1} = -p_1(x_1). \tag{6.16}$$

A similar approach can be applied to transverse force and moment equilibrium. The left portion of fig. 6.3 depicts the transverse loads and bending moments acting on an infinitesimal slice of the beam, focusing on plane $(\bar{\imath}_1, \bar{\imath}_2)$ in the left figure. Summation of the forces acting along axis $\bar{\imath}_2$ gives the transverse equilibrium equation

$$\frac{\mathrm{d}V_2}{\mathrm{d}x_1} = -p_2(x_1). \tag{6.17}$$

Summation of the moments taken about the centroidal axis $\bar{\imath}_3$ yields

$$\frac{\mathrm{d}M_3}{\mathrm{d}x_1} + V_2 = -q_3(x_1) + x_{2a}p_1(x_1), \tag{6.18}$$

where the last term arises because the line of action of the axial load, $p_1(x_1)$, passes through a point of coordinates (x_{2a}, x_{3a}). In general, there is no reason to believe that $x_{2a} = x_{3a} = 0$, *i.e.*, that the line of action of the applied axial load passes through the origin of the axis system, which is selected to coincide with the centroid of the section. For instance, if the axial load is the centrifugal force acting on the cross-section of a spinning beam, this axial load will be applied at the center of mass of the section, which might not coincide with its centroid.

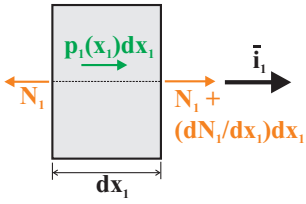

Fig. 6.2. Free body diagram for the axial forces.

Similarly, the right portion of fig. 6.3 depicts the transverse loads and bending moments acting on an infinitesimal slice of the beam, but now focusing on plane $(\bar{\imath}_1, \bar{\imath}_3)$. Summing the forces along axis $\bar{\imath}_3$ gives the second transverse equilibrium equation

$$\frac{\mathrm{d}V_3}{\mathrm{d}x_1} = -p_3(x_1), \tag{6.19}$$

and summing the moments about the centroidal axis $\bar{\imath}_2$ leads to

$$\frac{\mathrm{d}M_2}{\mathrm{d}x_1} - V_3 = -q_2(x_1) - x_{3a}p_1(x_1), \tag{6.20}$$

where x_{3a} defines the location at which the axial force p_1 acts on the cross-section.

The shear forces, V_2 and V_3, can be eliminated from the equilibrium equations by taking a derivative of eqs. (6.20) and (6.18), then introducing eqs. (6.19) and (6.17), respectively, to yield the equilibrium equations

$$\frac{\mathrm{d}^2M_2}{\mathrm{d}x_1^2} = -p_3(x_1) - \frac{\mathrm{d}}{\mathrm{d}x_1}[x_{3a}p_1(x_1) + q_2(x_1)], \tag{6.21a}$$

$$\frac{\mathrm{d}^2M_3}{\mathrm{d}x_1^2} = \quad p_2(x_1) + \frac{\mathrm{d}}{\mathrm{d}x_1}[x_{2a}p_1(x_1) - q_3(x_1)]. \tag{6.21b}$$

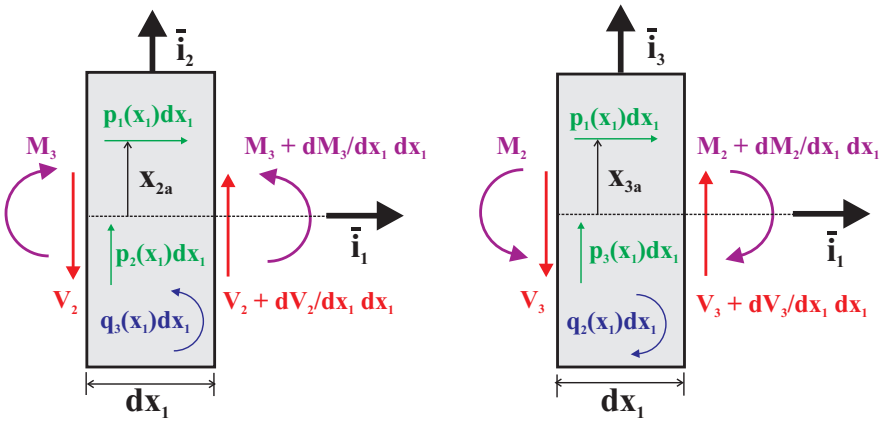

Fig. 6.3. Free body diagram for the transverse shear forces and bending moments. Left figure: view of the $(\bar{\imath}_1, \bar{\imath}_2)$ plane; right figure: view of the $(\bar{\imath}_1, \bar{\imath}_3)$ plane;

6.4 Governing equations

The governing equations for the beam transverse displacement field can be formulated as second order differential equations by introducing eqs. (5.6) into the sectional constitutive laws, eqs. (6.12) to find

$$\begin{aligned} H^c_{23}\frac{\mathrm{d}^2\bar{u}_2}{\mathrm{d}x_1^2} + H^c_{22}\frac{\mathrm{d}^2\bar{u}_3}{\mathrm{d}x_1^2} &= -M_2(x_1), \\ H^c_{33}\frac{\mathrm{d}^2\bar{u}_2}{\mathrm{d}x_1^2} + H^c_{23}\frac{\mathrm{d}^2\bar{u}_3}{\mathrm{d}x_1^2} &= \quad M_3(x_1). \end{aligned} \tag{6.22}$$

These differential equations can be used to solve for the beam transverse displacement field when the bending moments, $M_2(x_1)$ and $M_3(x_1)$, are known. For isostatic problems, the bending moment distribution can be expressed in terms of the externally applied loads based on equilibrium considerations alone.

For hyperstatic problems, another approach is necessary. Fourth order differential equations are obtained by introducing the sectional constitutive laws, eqs. (6.12), into the equilibrium equations, eqs. (6.16), (6.21a), and (6.21b), and then using the definition of the sectional strains, eq. (5.6), to find

$$\frac{\mathrm{d}}{\mathrm{d}x_1}\left[S\frac{\mathrm{d}\bar{u}_1}{\mathrm{d}x_1}\right] = -p_1, \tag{6.23a}$$

$$\frac{\mathrm{d}^2}{\mathrm{d}x_1^2}\left[H^c_{33}\frac{d^2\bar{u}_2}{\mathrm{d}x_1^2} + H^c_{23}\frac{\mathrm{d}^2\bar{u}_3}{\mathrm{d}x_1^2}\right] = p_2 + \frac{\mathrm{d}}{\mathrm{d}x_1}[x_{2a}p_1 - q_3], \tag{6.23b}$$

$$\frac{\mathrm{d}^2}{\mathrm{d}x_1^2}\left[H^c_{23}\frac{d^2\bar{u}_2}{\mathrm{d}x_1^2} + H^c_{22}\frac{\mathrm{d}^2\bar{u}_3}{\mathrm{d}x_1^2}\right] = p_3 + \frac{\mathrm{d}}{\mathrm{d}x_1}[x_{3a}p_1 + q_2]. \tag{6.23c}$$

These are second and fourth order, ordinary differential equations and their solution requires specification of a number of boundary conditions on $\bar{u}_1$, $\bar{u}_2$, and $\bar{u}_3$.

Using the beam example shown in fig. 6.1, the boundary conditions at the root of the beam are purely geometric,

$$\bar{u}_1 = \bar{u}_2 = \bar{u}_3 = 0, \quad \frac{\mathrm{d}\bar{u}_2}{\mathrm{d}x_1} = \frac{\mathrm{d}\bar{u}_3}{\mathrm{d}x_1} = 0, \tag{6.24}$$

which correspond to zero displacements and slopes at the clamped end. At the tip of the beam, the boundary conditions deal with the applied tip shear and axial loads, and bending moments

$$N_1 = P_1,\ M_3 = Q_3 - x_{2a}P_1,\ M_2 = Q_2 + x_{3a}P_1,\ V_2 = P_2,\ V_3 = P_3. \tag{6.25}$$

These boundary conditions must now be expressed in terms of the displacement components, $\bar{u}_1$, $\bar{u}_2$, and $\bar{u}_3$. Introducing the sectional constitutive laws, eq. (6.12), into eq. (6.25) and using the definition of the sectional strains, eq. (5.6), yields the boundary conditions expressed in terms of displacements as

$$\begin{aligned}
S\frac{\mathrm{d}\bar{u}_1}{\mathrm{d}x_1} &= P_1, \\
H^c_{33}\frac{\mathrm{d}^2\bar{u}_2}{\mathrm{d}x_1^2} + H^c_{23}\frac{\mathrm{d}^2\bar{u}_3}{\mathrm{d}x_1^2} &= \quad Q_3 - x_{2a}P_1, \\
H^c_{23}\frac{\mathrm{d}^2\bar{u}_2}{\mathrm{d}x_1^2} + H^c_{22}\frac{\mathrm{d}^2\bar{u}_3}{\mathrm{d}x_1^2} &= -Q_2 - x_{3a}P_1, \\
-\frac{\mathrm{d}}{\mathrm{d}x_1}\left[H^c_{33}\frac{\mathrm{d}^2\bar{u}_2}{\mathrm{d}x_1^2} + H^c_{23}\frac{\mathrm{d}^2\bar{u}_3}{\mathrm{d}x_1^2}\right] &= P_2 - [x_{2a}p_1 - q_3]_L, \\
-\frac{\mathrm{d}}{\mathrm{d}x_1}\left[H^c_{23}\frac{\mathrm{d}^2\bar{u}_2}{\mathrm{d}x_1^2} + H^c_{22}\frac{\mathrm{d}^2\bar{u}_3}{\mathrm{d}x_1^2}\right] &= P_3 - [x_{3a}p_1 + q_2]_L.
\end{aligned} \tag{6.26}$$

In summary, the governing equations of the problem are in the form of the three coupled differential equations (6.23a), (6.23b), and (6.23c) for the three sectional displacements $\bar{u}_1$, $\bar{u}_2$, and $\bar{u}_3$. The equations are second order in the axial displacement $\bar{u}_1$, and fourth order in the transverse displacements $\bar{u}_2$, and $\bar{u}_3$. There are ten associated boundary conditions, five at each end of the beam, as specified in eqs (6.24) and (6.26). Boundary conditions corresponding to various end configurations can be easily derived, as described in section 5.5.4.

6.5 Decoupling the three-dimensional problem

The governing equations described in the previous section form a set of coupled differential equations, and as such, are more difficult to solve than the bending problems presented in chapter 5. The axial behavior, eq. (6.23a), is decoupled from the bending behavior governed by eqs. (6.23b) and (6.23c), hence, these two problems can be handled separately. The bending equations (6.23b) and (6.23c), however, are coupled

and must be solved simultaneously. Stated in another way, the coupling between the two bending equations means that loads applied along axis $\bar{\imath}_2$ will not only cause deflection in that direction but can also produce deflection along axis $\bar{\imath}_3$.

The theory developed in the previous section requires the *axis system to be centroidal*, that is that axis $\bar{\imath}_1$ passes through the centroid of the cross-section. Although this choice decouples the axial behavior from bending, if an axial force is not applied at the centroid, it will contribute to the bending problem: see the terms $x_{2a}p_1$ and $x_{3a}p_1$, in eqs. (6.23b) and (6.23c), respectively. Similar contributions appear in the boundary conditions.

An important case of axial forces not applied at the centroid is found in air vehicles such as helicopters. The large centrifugal force generated by the rotation of the blade is an axial force *applied at the sectional center of mass*, which is, in general, distinct from its centroid. In such a case, $p_1(x_1)$ is the distributed centrifugal force applied on the blade, and (x_{2a}, x_{3a}) the coordinates of the sectional center of mass in a centroidal axis system. If a non-centroidal axis system is chosen, the resulting equations are considerably more complicated to solve, and in addition, the results are harder to understand and interpret.

6.5.1 Definition of the principal axes of bending

The question to be raised in this section is whether the governing equations can be further simplified by a judicious choice of the orientation of the centroidal axis system. The coupling between displacement components $\bar{u}_2$ and $\bar{u}_3$ in eqs. (6.23b) and (6.23c) arises from the presence of the cross bending stiffness coefficient, H^c_{23}, defined in eq. (6.9). This term can be made to vanish by an appropriate choice of the orientation or rotation of axes $\bar{\imath}_2$ and $\bar{\imath}_3$, within the plane of the cross-section. The *principal centroidal axes of bending* are defined as a set of axes with their origin at the centroid of the section and for which

$$H^c_{23} = \int_{\mathcal{A}} E x_2 x_3 \, \mathrm{d}\mathcal{A} = 0. \tag{6.27}$$

The actual procedure for determining the orientation of the principal centroidal axes of bending is described in section 6.6. The result is a new axis system, $\mathcal{I}^* = (\bar{\imath}^*_2, \bar{\imath}^*_3)$, that is rotated about the axis of the beam, $\bar{\imath}_1$, *i.e.*, leaving the axis of the beam unchanged, $\bar{\imath}_1 = \bar{\imath}^*_1$. The notation $(\cdot)^*$ will be used to indicate quantities resolved in the new reference frame.

In this frame of reference, the constitutive laws for the cross-section, eq. (6.13), take the following, fully decoupled form

$$\bar{\epsilon}^*_1 = \frac{N^*_1}{S^*}, \quad \kappa^*_2 = \frac{M^*_2}{H^{c*}_{22}}, \quad \kappa^*_3 = \frac{M^*_3}{H^{c*}_{33}}. \tag{6.28}$$

The corresponding axial stress distribution, eq. (6.3), becomes

$$\sigma^*_1 = E\left[\frac{N^*_1}{S^*} + x^*_3 \frac{M^*_2}{H^{c*}_{22}} - x^*_2 \frac{M^*_3}{H^{c*}_{33}}\right], \tag{6.29}$$

which is considerably simpler than eq. (6.14).

6.5.2 Decoupled governing equations

The use of the principal centroidal axis of bending also simplifies the governing equations of the problem, eqs. (6.23a) to 6.23c, which now decouple into *three independent equations* that describe the axial and bending behaviors of the beam. With reference to the particular beam configuration illustrated in fig. 6.1, three independent problems are now defined.

The axial problem

The axial problem is governed by eq. (6.23a), which now takes on the following form

$$\frac{\mathrm{d}}{\mathrm{d}x_1^*}\left[S^*\frac{\mathrm{d}\bar{u}_1^*}{\mathrm{d}x_1^*}\right] = -p_1^*. \tag{6.30}$$

For the problem shown in fig. 6.1, the boundary conditions are as follows: $\bar{u}_1^* = 0$ at the root of the beam, whereas at its tip, $S^*\mathrm{d}\bar{u}_1^*/\mathrm{d}x_1^* = P_1^*$. This extensional problem is identical to that discussed in section 5.4. Note that $S = S^*$ since the axial stiffness remains unaffected by a rotation of axes $\bar{\imath}_2$ and $\bar{\imath}_2$ about axis $\bar{\imath}_1$.

The first bending problem

The bending problem reduces to two independent equations. The first of these, eq. (6.23b), takes the following form

$$\frac{\mathrm{d}^2}{\mathrm{d}x_1^{*2}}\left[H_{33}^{c*}\frac{\mathrm{d}^2\bar{u}_2^*}{\mathrm{d}x_1^{*2}}\right] = p_2^* + \frac{\mathrm{d}}{\mathrm{d}x_1^*}[x_{2a}^* p_1^* - q_3^*], \tag{6.31}$$

which describes bending in plane $(\bar{\imath}_1^*, \bar{\imath}_2^*)$. This differential equation is subject to the following boundary conditions at the beam's root $\bar{u}_2^* = 0$ and $\mathrm{d}\bar{u}_2^*/\mathrm{d}x_1^* = 0$ and at its tip,

$$H_{33}^{c*}\frac{\mathrm{d}^2\bar{u}_2^*}{\mathrm{d}x_1^{*2}} = Q_3^* - x_{2a}^* P_1^*, \quad -\frac{\mathrm{d}}{\mathrm{d}x_1^*}\left[H_{33}^{c*}\frac{\mathrm{d}^2\bar{u}_2^*}{\mathrm{d}x_1^{*2}}\right] = P_2^* - [x_{2a}^* p_1^* - q_3^*].$$

The second bending problem

Finally, eq. (6.23c) takes the following form

$$\frac{\mathrm{d}^2}{\mathrm{d}x_1^{*2}}\left[H_{22}^{c*}\frac{\mathrm{d}^2\bar{u}_3^*}{\mathrm{d}x_1^{*2}}\right] = p_3^* + \frac{\mathrm{d}}{\mathrm{d}x_1^*}[x_{3a}^* p_1^* + q_2^*], \tag{6.32}$$

which describes bending in plane $(\bar{\imath}_1, \bar{\imath}_3^*)$. The differential equation is subject to the following boundary conditions at the beam's root $\bar{u}_3^* = 0$ and $\mathrm{d}\bar{u}_3^*/\mathrm{d}x_1^* = 0$ and at its tip,

$$H_{22}^{c*}\frac{\mathrm{d}^2\bar{u}_3^*}{\mathrm{d}x_1^{*2}} = -Q_2^* - x_{3a}^* P_1^*, \quad -\frac{\mathrm{d}}{\mathrm{d}x_1^*}\left[H_{22}^{c*}\frac{\mathrm{d}^2\bar{u}_3^*}{\mathrm{d}x_1^{*2}}\right] = P_3^* - [x_{3a}^* p_1^* + q_2^*].$$

Note that the two bending problems are identical problems written in the two orthogonal planes defined by the principal centroidal axes of bending. Each bending problem is identical to the bending problems discussed in section 5.5. It is clear that the rotation of the axes to the principal directions takes place about axis $\bar{\imath}_1$. Hence, $\bar{\imath}_1^* = \bar{\imath}_1$, $x_1^* = x_1$, and $\bar{u}_1^* = \bar{u}_1$. The notational difference is made to emphasize the fact that all quantities in the decoupled equations are resolved along the principal centroidal axes of bending.

6.6 The principal centroidal axes of bending

Consider an arbitrary set of axes, $\mathcal{I} = (\bar{\imath}_2, \bar{\imath}_3)$, with their origin at the centroid of the section, as depicted in fig. 6.4. Next, a new set of axes, $\mathcal{I}^* = (\bar{\imath}_2^*, \bar{\imath}_3^*)$, is defined by rotating the first set of axes by an angle α. Let (x_2, x_3) and (x_2^*, x_3^*) denote the coordinates of point **P** resolved in coordinate systems $\mathcal{I}$ and $\mathcal{I}^*$, respectively.

Coordinate transformations are discussed in appendix A.3.4, and the two sets of coordinates, (x_2, x_3) and (x_2^*, x_3^*), are related by eq. (A.43). The centroidal bending stiffnesses in system $\mathcal{I}^*$ can be computed using eq. (6.8) to find

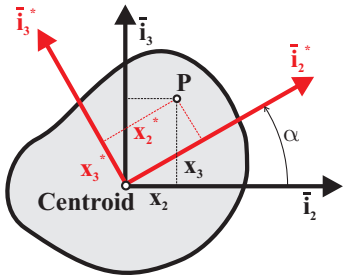

Fig. 6.4. Rotation of the axes of the cross-section.

$$H_{22}^{c*} = \int_{\mathcal{A}} E\,(-x_2\sin\alpha + x_3\cos\alpha)^2\,\mathrm{d}\mathcal{A},$$
$$H_{33}^{c*} = \int_{\mathcal{A}} E\,(x_2\cos\alpha + x_3\sin\alpha)^2\,\mathrm{d}\mathcal{A},$$
$$H_{23}^{c*} = \int_{\mathcal{A}} E\,(x_2\cos\alpha + x_3\sin\alpha)(-x_2\sin\alpha + x_3\cos\alpha)\,\mathrm{d}\mathcal{A}.$$

Expanding these expressions, and noting that centroidal axes are being used, gives

$$H_{22}^{c*} = H_{22}^c\cos^2\alpha + H_{33}^c\sin^2\alpha - 2H_{23}^c\sin\alpha\cos\alpha, \tag{6.33a}$$
$$H_{33}^{c*} = H_{22}^c\sin^2\alpha + H_{33}^c\cos^2\alpha + 2H_{23}^c\sin\alpha\cos\alpha, \tag{6.33b}$$
$$H_{23}^{c*} = (H_{22}^c - H_{33}^c)\sin\alpha\cos\alpha + H_{23}^c(\cos^2\alpha - \sin^2\alpha). \tag{6.33c}$$

With the help of basic double-angle trigonometric identities, these expressions can be rewritten as

$$H_{22}^{c*} = \frac{H_{22}^c + H_{33}^c}{2} + \frac{H_{22}^c - H_{33}^c}{2}\cos 2\alpha - H_{23}^c \sin 2\alpha; \tag{6.34a}$$

$$H_{33}^{c*} = \frac{H_{22}^c + H_{33}^c}{2} - \frac{H_{22}^c - H_{33}^c}{2}\cos 2\alpha + H_{23}^c \sin 2\alpha; \tag{6.34b}$$

$$H_{23}^{c*} = + \frac{H_{22}^c - H_{33}^c}{2}\sin 2\alpha + H_{23}^c \cos 2\alpha. \tag{6.34c}$$

Note the very close similarity between these equations, expressing the relationship between bending stiffnesses in two different coordinate system and eqs. (1.49) expressing the relationship between stress components in two different coordinate systems, or eqs. (1.94) expressing the relationship between strain components in two different coordinate systems. This is due to the fact that bending stiffnesses, stress components, and strain components, all form *second order tensors*. The components of second order tensors under an axis rotation all behave in the same manner, as expressed by eqs. (6.34), (1.49), or (1.94).

By definition (6.27), the principal centroidal axes of bending are such that $H_{23}^{*c} = 0$. Equation (6.34c) yields the following equation for the orientation of the principal axes

$$\tan 2\alpha^* = \frac{2H_{23}^c}{H_{33}^c - H_{22}^c}. \tag{6.35}$$

This equation presents two solutions, α^* and $\alpha^* + \pi/2$, corresponding to two mutually orthogonal principal centroidal axes directions. The maximum bending is found about one direction, and the minimum about the other. To define these orientations unequivocally, it is convenient to separately define the sine and cosines of angle $2\alpha^*$ as follows

$$\sin 2\alpha^* = \frac{H_{23}^c}{\Delta} \quad \text{and} \quad \cos 2\alpha^* = \frac{H_{33}^c - H_{22}^c}{2\Delta}, \tag{6.36}$$

where

$$\Delta = \sqrt{\left(\frac{H_{33}^c - H_{22}^c}{2}\right)^2 + (H_{23}^c)^2}. \tag{6.37}$$

This result is equivalent to eq. (6.35), but it gives a unique solution for α^* because both the sine and cosine of the angle are known. The minimum and maximum bending stiffnesses, denoted H_{22}^{c*} and H_{33}^{c*}, respectively, act about the directions α^* and $\alpha^* + \pi/2$, respectively. These minimum and maximum bending stiffnesses, called *principal centroidal bending stiffnesses*, are evaluated by introducing the orientation of the principal axes, eq. (6.36), into eqs. (6.34a) and (6.34b), to find

$$H_{22}^{c*} = \frac{H_{33}^c + H_{22}^c}{2} - \Delta; \quad H_{33}^{c*} = \frac{H_{33}^c + H_{22}^c}{2} + \Delta. \tag{6.38}$$

In summary, the orientation of the principal centroidal axes of bending is obtained according to the following procedure.

1. Compute the centroid of the section using the definition, eq. (6.11);
2. Compute the bending stiffnesses in this axis system using eqs. (6.8) and (6.9);
3. Compute the orientation of the principal axes of bending using eq. (6.36);

4. Compute the principal bending stiffnesses using eq. (6.38).

It is interesting to note that the principal axes of bending are axes about which the bending stiffnesses are extremal: minimum about $\bar{\imath}_2^*$, and maximum about $\bar{\imath}_3^*$. Indeed, the bending stiffness is expressed in terms of α^* in eq. (6.34a): the minimum value of $H_{22}^{c*}(\alpha^*)$ occurs when its derivative with respect to α^* vanishes

$$\frac{\mathrm{d}H_{22}^{c*}}{\mathrm{d}\alpha^*} = \frac{H_{33}^c - H_{22}^c}{2}\, 2\sin 2\alpha^* - H_{23}^c\, 2\cos 2\alpha^* = 0. \tag{6.39}$$

This condition is identical to eq. (6.35). Similarly, the value of α^* which maximizes $H_{33}^{c*}(\alpha^*)$ is the same value determined by eq. (6.35). In summary, the principal axes of bending are such that H_{23}^{*c} vanishes, and the corresponding bending stiffnesses are extremal.

6.6.1 The bending stiffness ellipse

It is noted in the previous section that bending stiffnesses, stress components, and strain components, all form second order tensors, and the components of second order tensors under an axis rotation all behave in the same manner, as expressed by eqs. (6.34), (1.49), or (1.94). Hence, it should not come as a surprise that Mohr's circle representation of stress components, as presented in section 1.3.6, or of strain components, as presented in section 1.6.4, can also be used to represent the bending stiffness components.

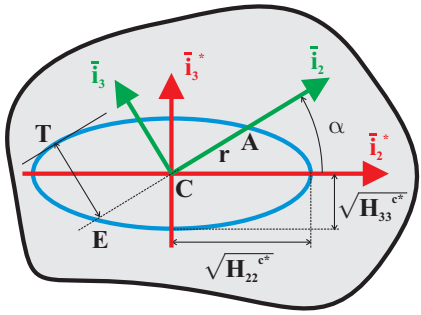

Fig. 6.5. The bending stiffness ellipse of a cross-section.

Bending stiffness components, however, afford another representation that is more informative than Mohr's circle. Figure 6.5 shows the arbitrarily shaped cross-section of a beam with its principal centroidal axes of bending, $\bar{\imath}_2^*$ and $\bar{\imath}_3^*$; point **C** is located at the centroid of the cross-section. An ellipse, called the *bending stiffness ellipse*, with semi-axes $\sqrt{H_{33}^{c*}}$ and $\sqrt{H_{22}^{c*}}$ is constructed with its center at the centroid of the section and its axes aligned with the principal centroidal axes of bending.

By construction, the equation of this ellipse is

$$\frac{x_2^{*2}}{H_{22}^{c*}} + \frac{x_3^{*2}}{H_{33}^{c*}} = 1. \tag{6.40}$$

Consider now an arbitrary axis system, $\mathcal{I} = (\bar{\imath}_2, \bar{\imath}_3)$, where $\bar{\imath}_2$ forms an angle α with respect to axis $\bar{\imath}_2^*$. Let point **A** be located at the intersection of axis $\bar{\imath}_2$ with the bending stiffness ellipse. The coordinates of point **A** are $x_2^* = r\cos\alpha$ and $x_3^* = r\sin\alpha$, where r is the length of segment **CA**. Since point **A** is on the bending stiffness ellipse, it

follows that eq. (6.40) can be rewritten as $r^2(\cos^2\alpha/H_{33}^{c*} + \sin^2\alpha/H_{22}^{c*}) = 1$, and hence,

$$r^2 = \frac{H_{22}^{c*}H_{33}^{c*}}{H_{22}^{c*}\cos^2\alpha + H_{33}^{c*}\sin^2\alpha} = \frac{H_{22}^{c*}H_{33}^{c*}}{H_{22}^{c}},$$

where the last equality results from eq. (6.33a). A fundamental property of an ellipse is that the product of the lengths of segments **TE** and **CA** equals the product of the lengths of the semi-axes, *i.e.*, $r\ \mathbf{TE} = \sqrt{H_{22}^{c*}H_{33}^{c*}}$. Introducing the value of r computed above leads to

$$\mathbf{TE}^2 = H_{22}^{c}. \tag{6.41}$$

The interpretation of this result is as follows: the bending stiffness of the cross-section about an arbitrary axis $\bar{\imath}_2$ equals the square of the distance between this axis and the tangent to the bending stiffness ellipse that is parallel to $\bar{\imath}_2$. As axis $\bar{\imath}_2$ rotates around the centroid, the bending stiffness ellipse provides a convenient visualization of the variation of the bending stiffness about this axis.

6.7 The neutral axis

If the cross-section of the beam is made of a homogeneous material, the axial stress distribution varies linearly over the cross-section. Indeed, the axial stress distribution described by eq. (6.14) is the equation of a plane with terms in x_2, x_3, and an independent term. The same observation can be made by considering the distribution of axial stress expressed in principal centroidal axes of bending, see eq. (6.29). If the material Young's modulus is a function of position over the cross-section, *i.e.*, if $E = E(x_2, x_3)$, as would be the case for a beam made of layered composite material, the axial stress distribution over the cross-section is no longer linear.

For sections made of homogeneous material, three distinct types of the axial stress distribution are possible over the cross-section.

1. If the *axial force, N_1, has a sufficiently large tensile (positive) value*, the axial stress is tensile over the entire cross-section.
2. If the *axial force, N_1, has a sufficiently large compressive (negative) value*, the axial stress is compressive over the entire cross-section.
3. If the *axial force, N_1, assumes an intermediate value or vanishes*, the axial stress will vanish along a straight line intersecting the boundaries of the cross-section; the axial stress will be tensile on one side of this line and compressive on the other. The locus of zero axial stress is a straight line called the *neutral axis*.

Figure 6.6 illustrates the concept of the neutral axis, which divides the cross-section into two regions, one subjected to compressive stresses, the other to tensile stresses. Along the neutral axis, the axial stress vanishes, while along lines parallel to the neutral axis, the axial stress is constant. Consequently, axial stresses will increase or decrease most rapidly when moving along the direction perpendicular to the neutral axis: the maximum axial stress gradient direction is normal to the neutral axis. It then follows that the extremal values of the axial stress are found at the points of the cross-section that are at the largest perpendicular distance from the neutral axis, as

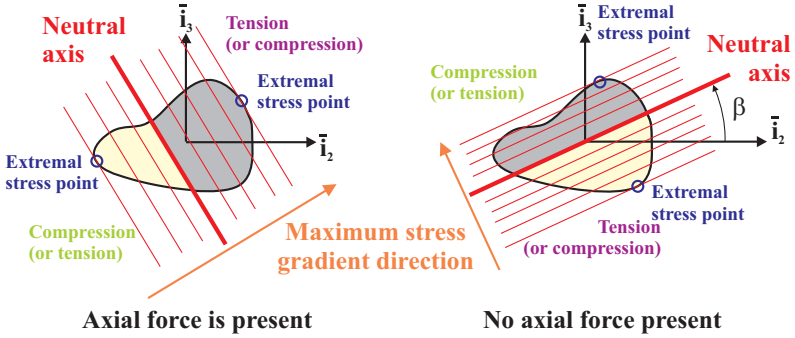

Fig. 6.6. Neutral axis on a cross-section: left portion, axial force is preset, right portion, the axial force vanishes. Along the red lines, the axial stresses remain constants.

illustrated in fig. 6.6. The neutral axis is an important concept that helps with visualizing the axial stress field over a cross-section subjected to axial forces and bending moments. It also facilitates the determination of the locations of the extremal axial stresses on the cross-section.

The neutral axis is a straight line, and its equation is readily found by imposing the vanishing of the axial stress in eq. (6.14) to find

$$\frac{N_1}{S} + \frac{H^c_{33}M_2 + H^c_{23}M_3}{\Delta_H}\, x_3 - \frac{H^c_{23}M_2 + H^c_{22}M_3}{\Delta_H}\, x_2 = 0. \tag{6.42}$$

Clearly, this is the equation of a line in the plane of the cross-section for a given axial force, N_1, and bending moments, M_2 and M_3. The slope of this line is found as

$$\tan\beta = \frac{x_3}{x_2} = \frac{H^c_{23}M_2 + H^c_{22}M_3}{H^c_{33}M_2 + H^c_{23}M_3}. \tag{6.43}$$

It is often convenient to work with the principal centroidal axes of bending. In that case, the equation of the neutral axis is found by imposing the vanishing of the axial stress in eq. (6.29) to find

$$\frac{N^*_1}{S^*} + x^*_3\,\frac{M^*_2}{H^{c*}_{22}} - x^*_2\,\frac{M^*_3}{H^{c*}_{33}} = 0. \tag{6.44}$$

The slope of the neutral axis is simply $\tan\beta^* = x^*_3/x^*_2 = (H^{c*}_{22}M^*_3)/(H^{c*}_{33}M^*_2)$.

As illustrated in fig. 6.6, when the axial force vanishes, the neutral axis passes through the origin of the axis system, which coincides with the centroid of the section.

Example 6.1. Relationship between the bending stiffness ellipse and the neutral axis

Consider a cross-section of arbitrary shape subjected to a bending moment of magnitude M, as depicted in fig. 6.7. Axes $\bar{\imath}^*_1$ and $\bar{\imath}^*_2$ are the principal centroidal axes

of bending of the cross-section and the bending stiffness ellipse, as defined in section 6.6.1, has also been drawn on the figure. The bending moment vector is oriented at an angle γ^* with axis $\bar{\imath}_2^*$. Find the location of the neutral axis and of the maximum axial stresses in the section.

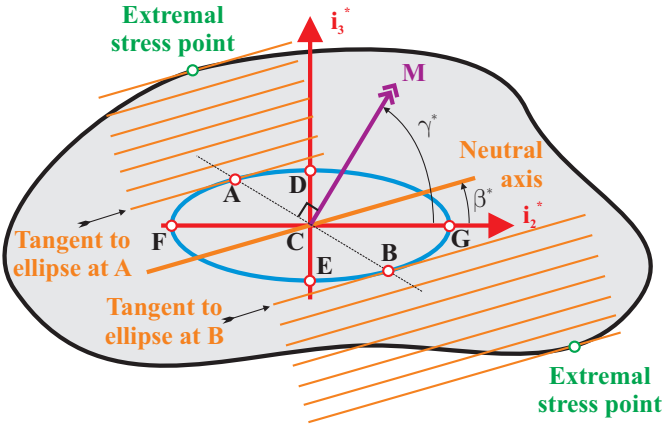

Fig. 6.7. Cross-section subjected to a bending moment, M.

Since axes $\bar{\imath}_1^*$ and $\bar{\imath}_2^*$ are the principal centroidal axes of bending of the cross-section, the distribution of axial stress is given by eq. (6.29) as $\sigma_1^*/E = x_3^*\ M_2^*/H_{22}^{c*} - x_2^*\ M_3^*/H_{33}^{c*}$. Clearly, $M_2^* = M\cos\gamma^*$ and $M_3^* = M\sin\gamma^*$, leading to the following distribution of axial stress, $\sigma_1^*/E = M(x_3^*\cos\gamma^*/H_{22}^{c*} - x_2^*\sin\gamma^*/H_{33}^{c*})$. The orientation of the neutral axis is

$$\tan\beta^* = \frac{x_3^*}{x_2^*} = \frac{H_{22}^{c*}}{H_{33}^{c*}}\tan\gamma^*.$$

This result implies that angles γ^* and β^* are, in general, not equal. Two notable exceptions exist: if $\gamma^* = 0$ or $\pi/2$, $\beta^* = 0$ or $\pi/2$, respectively. Because the selected axes are principal centroidal axes of bending, $\gamma^* = 0$ or $\pi/2$ implies that the bending moment is applied about one of the principal centroidal axes of bending directions, and its direction then coincides with that of the neutral axis. The other exception is when $H_{22}^{c*} = H_{33}^{c*}$, in which case any axis system with its origin at the centroid is a principal centroidal axis of bending system.

In summary, the direction of the neutral axis coincides with that of the applied bending moment if and only if the applied bending moment acts about a principal centroidal axes of bending direction.

The equation of the bending stiffness ellipse is given by eq. (6.40), and it is easy to show that the equation of the tangent to the ellipse at one of its points, **A**, with coordinates (x_{2A}, x_{3A}), is $x_2^* x_{2A}/H_{33}^{c*} + x_3^* x_{3A}/H_{22}^{c*} = 1$. Now, let points **A** and **B** be the intersections of the normal to the moment vector with the bending stiffness ellipse, as shown in fig. 6.7. The coordinates of point **A** become $x_{2A} = -\mathbf{AC}\sin\gamma^*$

and $x_{3A} = \mathbf{AC}\cos\gamma^*$, and the equation of the tangent to the ellipse at point **A** becomes $x_2^* \sin\gamma^*/H_{33}^{c*} + x_3^* \cos\gamma^*/H_{22}^{c*} = 1/\mathbf{AC}$. Clearly, the slope of this tangent is

$$\frac{x_3^*}{x_2^*} = \frac{H_{22}^{c*}}{H_{33}^{c*}} \tan\gamma^*.$$

The *slope of this tangent is identical to that of the neutral axis*. Hence, the neutral axis is parallel to the tangent to the bending stiffness ellipse at point **A**.

The orientation of the neutral axis as the orientation of the applied bending moment vector changes is now easily visualized. First, let the direction of the applied bending moment coincide with the principal direction $\overline{\imath}_2^*$, *i.e.*, $\gamma^* = 0$. The neutral axis is parallel to the tangent to the ellipse at points **D** or **E**, *i.e.*, it coincides with axis $\overline{\imath}_2^*$. Similarly, if the direction of the applied bending moment coincides with the principal direction $\overline{\imath}_3^*$, the neutral axis coincides again with $\overline{\imath}_3^*$. If the bending stiffness ellipse is very elongated, *i.e.*, if $H_{33}^{c*} \gg H_{22}^{c*}$, very rapid variations of the orientation of the neutral axis must be expected because of the very rapid variation of the tangent to the bending stiffness ellipse about points **F** or **G**.

Finally, as explained in section 6.7, the orientation of the neutral axis gives the direction of the maximum axial stress gradient and the location of the maximum axial stress in the cross-section, as illustrated in fig. 6.7.

Example 6.2. Maximum bending moments for rectangular section

Consider a solid rectangular section of width b and height h subjected to an axial force, N_1, and bending moments, M_2 and M_3, as depicted in fig. 6.8. If the material has a yield strain ϵ_y, find the yield envelope for the section. In view of the symmetry of the cross-section, the axes shown in fig. 6.8 are the principal centroidal axes of bending.

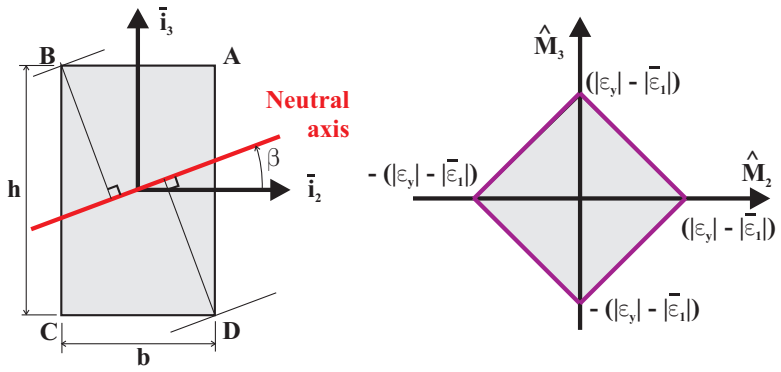

Fig. 6.8. Left figure: neutral axis for a rectangular section. Right figure: yield envelope for the rectangular section under combined bending moment and axial force.

First, assume that no axial force is applied to the section and that the applied bending moments give the neutral axis depicted in fig. 6.8. The extremal axial

stresses will occur at the largest normal distance from the neutral axis, *i.e.*, at the corners of the section, points **B** and **D**. Note that for $0 < \beta^* < \pi/2$, points **B** and **D** remain the locations of the extremal stresses. On the other hand, for $-\pi/2 < \beta^* < 0$, the extremal axial stresses will occur at the other two corners of the section, points **A** and **C**. Note that $\beta^* = 0$ or $\beta^* = \pi/2$ are special cases: the extremal stresses are found along edge **AB** and **CD** or **BC** and **DA**, respectively. If an axial force is present, a *uniform axial stress* is added to the axial stress distribution due to the bending moments, but this does not affect the location of the extremal axial stresses. Clearly, yielding will initiate at one of the four corner points **A**, **B**, **C**, or **D**.

In view of eq. (6.29), the non-dimensional axial stress distribution can be written as

$$\begin{aligned}\frac{\sigma_1}{E} &= \frac{N_1}{S} + \frac{M_2}{H^c_{22}}\, x_3 - \frac{M_3}{H^c_{33}}\, x_2 \\ &= \frac{N_1}{S} + \frac{hM_2}{2H^c_{22}}\,\frac{2x_3}{h} - \frac{bM_3}{2H^c_{33}}\,\frac{2x_2}{b} = \bar{\epsilon}_1 + \bar{M}_2\bar{x}_3 - \bar{M}_3\bar{x}_2,\end{aligned}$$

where $\bar{M}_2 = hM_2/(2H^c_{22})$ and $\bar{M}_3 = bM_3/(2H^c_{33})$ are the non-dimensional bending moment, and $\bar{x}_2 = 2x_2/b$ and $\bar{x}_3 = 2x_3/h$ the non-dimensional coordinates.

The yield criterion is $\sigma_1/E = \epsilon_y$, which must be applied at points **A**, **B**, **C**, and **D**, because the extremal stresses occur at those locations. These four yield conditions are summarized as

$$|\bar{M}_2 - \bar{M}_3| = |\epsilon_y| - |\bar{\epsilon}_1|, \quad |\bar{M}_2 + \bar{M}_3| = |\epsilon_y| - |\bar{\epsilon}_1|.$$

These conditions correspond to four line segments in the bending moment plane $(\bar{M}_2, \bar{M}_3)$ that define the diamond-shaped zone shown in fig. 6.8. The inside of the diamond corresponds to safe loading conditions, and the material starts to yield for loading conditions falling on the edges of the diamond. As the axial force and hence, axial strain increases, the size of the diamond shrinks, which indicates that smaller bending moments can be applied. When $\bar{\epsilon}_1 = \epsilon_y$, the material yields under the axial force alone, and no bending moments can be applied.

6.8 Evaluation of sectional stiffnesses

The determination of the orientation of the principal centroidal axes of bending requires the computation of sectional stiffnesses. This section presents a number of tools that will ease this task.

6.8.1 The parallel axis theorem

The bending stiffness of a section are sometimes to be computed with respect to two axis systems that are parallel to each other, but have a different origin, as illustrated in fig. 6.9. The bending stiffnesses of the section with respect to axes $\bar{\imath}_2$ and $\bar{\imath}^c_2$ will be denoted H_{22} and H^c_{22}, respectively; H^c_{22} is called the centroidal bending stiffness.

The *parallel axis theorem* relates the distinct bending stiffnesses computed with respect to parallel axes, one of them centroidal. Let d_3 be the distance between the parallel axes, $\bar{\imath}_2$ and $\bar{\imath}_2^c$.

Bending stiffness H_{22} is given by eq. (6.8) as

$$H_{22} = \int_{\mathcal{A}} E\,(d_3 + x_3^c)^2\,\mathrm{d}\mathcal{A},$$

where x_3^c is the coordinate of a point of the section measured in the centroidal system, $(\bar{\imath}_2^c, \bar{\imath}_3^c)$. Expanding this result then leads to

$$H_{22} = d_3^2 \left[\int_{\mathcal{A}} E\,\mathrm{d}\mathcal{A}\right] + 2d_3 \left[\int_{\mathcal{A}} E\,x_3^c\,\mathrm{d}\mathcal{A}\right] + \left[\int_{\mathcal{A}} E\,(x_3^c)^2\,\mathrm{d}\mathcal{A}\right].$$

The first bracketed term is the axial stiffness of the section, S, see eq. (6.5); the second bracketed term vanishes because axis $\bar{\imath}_2^c$ is centroidal, see eq. (6.5); finally, the last bracketed term is the centroidal bending stiffness defined by eq. (6.8). Hence, the result simplifies to $H_{22} = Sd_3^2 + H_{22}^c$. A similar process can be applied to the bending stiffness H_{33} and cross bending stiffness H_{23} to find

$$H_{22} = H_{22}^c + Sd_3^2; \quad H_{33} = H_{33}^c + Sd_2^2; \tag{6.45}$$

and

$$H_{23} = H_{23}^c + Sd_2d_3. \tag{6.46}$$

Because the second term on the right hand side of eqs. (6.45), called the "transport term," is *strictly positive*, it follows that $H_{22} > H_{22}^c$ and $H_{33} > H_{33}^c$, that is, the bending stiffness always increases when moving away from the centroid. In other words, the minimum bending stiffness is obtained when computed with respect to the centroid. On the other hand, the second term on the hand side of eq. (6.46) can be *positive or negative*: cross bending stiffnesses can increase or decrease when moving away from the centroid.

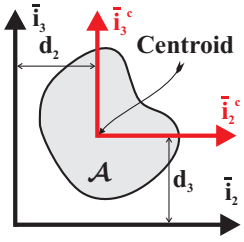

Fig. 6.9. Parallel axes.

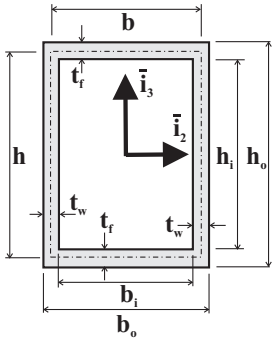

Fig. 6.10. Thin-walled rectangular section.

6.8.2 Thin-walled sections

Many beam sections involved aerospace structures are thin-walled sections, and this fact simplifies the evaluation of the bending stiffnesses. Consider the homogeneous, thin-walled rectangular box beam shown in fig. 6.10. Due to the symmetry of the section, the axes indicated on the figure are principal centroidal axes of bending. The inner and outer heights are h_i and h_o, respectively, whereas the inner and outer width are b_i and b_o, respectively. The thickness of the flange, t_f, and web, t_w, are written as $t_f = (h_o - h_i)/2$ and $t_w = (b_o - b_i)/2$, respectively. The height, h, and width, b, of the section, as measured from mid-wall lines are now $h = (h_o + h_i)/2$ and $b = (b_o + b_i)/2$.

These dimensions are the average height and width of the section. The bending stiffness of the section with respect to axis $\bar{\imath}_2$ can be computed by subtracting the bending stiffness of the inner rectangular area from that of the outer rectangular area to find

$$H_{22}^c = E\left(\frac{b_o h_o^3}{12} - \frac{b_i h_i^3}{12}\right), \tag{6.47}$$

where E is the material Young's modulus. This expression can be rewritten in terms of the average dimensions and wall thicknesses by noting that $b_o = b + t_w$, $b_i = b - t_w$, $h_o = h + t_f$, and $h_i = h - t_f$, to find

$$H_{22}^c = \frac{E}{12}\left[(b + t_w)(h + t_f)^3 - (b - t_w)(h - t_f)^3\right]. \tag{6.48}$$

Expanding the cubic power and regrouping terms then yields

$$H_{22}^c = \frac{E}{12}\left\{6bh^2 t_f\left[1 + \frac{1}{3}\left(\frac{t_f}{h}\right)^2\right] + 2h^3 t_w\left[1 + 3\left(\frac{t_f}{h}\right)\right]\right\}. \tag{6.49}$$

If the wall thickness is small, *i.e.*, $t_f/h \ll 1$, this term is negligible compared to unity, and the bending stiffness reduces to

$$H_{22}^c \approx E\left[2\frac{t_w h^3}{12} + 2bt_f\left(\frac{h}{2}\right)^2\right]. \tag{6.50}$$

The first term represents the bending stiffnesses of the left and right webs, computed with the average height h, whereas the last term gives the contribution of the top and bottom flanges using their average width b.

To better understand the meanings of these terms, consider the calculation of H_{22}^c directly from the individual components of the section. First, compute bending stiffness of the left and right webs about their centroids: $t_w h^3/12$ for each web. Next the contributions of the flanges are added: $(bt_f^3/12 + bt_f h^2/4)$ for each flange; the first term represents the bending stiffness of the flange with respect to its own centroid, and the second term is the transport term according to the parallel axis theorem, eq. (6.45). Adding up the contributions of the various components yields the bending stiffness of the section as

$$H^c_{22} = E\left[2\frac{t_w h^3}{12} + 2\left(\frac{bt_f^3}{12} + bt_f\left(\frac{h}{2}\right)^2\right)\right].$$

If the wall thicknesses satisfy the thin-wall assumption, *i.e.*, $t_f/h \ll 1$, terms containing higher powers of the wall thickness can be ignored, and the result is identical to that shown in eq. (6.50) above. A similar reasoning can be used to evaluate the bending stiffness, H^c_{33}.

6.8.3 Triangular area equivalence method

Consider the homogeneous triangular area depicted in fig. 6.11. It can be shown that all area moment calculations can be performed based on lumping the area of the triangle, $\mathcal{A}$, at three points located at the midpoint of each side of the triangle. In other words, the triangular area is replaced by three concentrated areas, each of area $\mathcal{A}/3$, located at the midpoint of each side of the triangle, as illustrated on the figure. The area moment are evaluated based on these lumped areas to find

$$I_{22} = \frac{\mathcal{A}}{3}\sum_{i=1}^{3} x_{3i}^2, \quad I_{33} = \frac{\mathcal{A}}{3}\sum_{i=1}^{3} x_{2i}^2, \quad I_{23} = \frac{\mathcal{A}}{3}\sum_{i=1}^{3} x_{2i}x_{3i}. \tag{6.51}$$

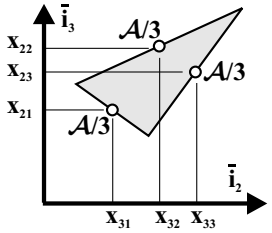

Fig. 6.11. Triangular area equivalent lumped areas.

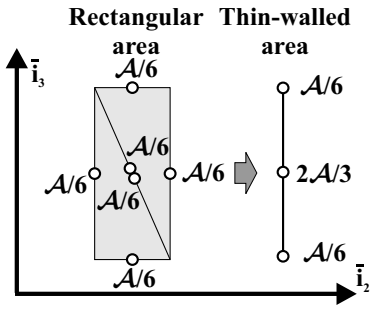

Fig. 6.12. Rectangular area equivalent lumped areas.

An important special case is the rectangular area which, as shown in fig. 6.12, can be decomposed into two triangular areas, each with one-half of the area of the rectangle. This yields an equivalent lumped model for the rectangle with lumped areas at the midpoints of each of its sides and a fifth at its center. A very useful result is obtained by letting the width of the rectangle decrease to a vanishingly small value while retaining the height and area (in other words, the thin-wall assumption). This case is shown on the right side of fig. 6.12. Now, the representation collapses to a one-dimensional line with lumped areas of $\mathcal{A}/6$ at each end and $2\mathcal{A}/3$ at the midpoint. This is a particularly useful representation for computing the centroids, area moments and bending stiffnesses for thin-walled sections.

6.8.4 Useful results

Thin rectangular strip

The left portion of fig. 6.13 shows a thin rectangular strip of thickness t and height h where $t \ll h$. The centroid of this strip is located at distances d_2 and d_3 from axes $\bar{\imath}_3$ and $\bar{\imath}_2$, respectively. The bending stiffnesses of this strip are approximated as

$$H_{22} = E\left(\frac{th^3}{12} + htd_3^2\right), \quad H_{33} = E\, htd_2^2, \quad H_{23} = E\, htd_2d_3. \tag{6.52}$$

These results are obtained by first computing the bending stiffness in the principal centroidal axes of the thin strip, then using the parallel axis theorem to translate the bending stiffnesses to the required axis. Terms containing higher powers of the thickness are neglected.

Rotated thin rectangular strip

Similar results can be obtained for the same rectangular strip rotated of an angle, α, with respect to the $\bar{\imath}_2$ axis shown in the right portion fig. 6.13

$$\begin{aligned} H_{22} &= E\left(\frac{th^3}{12}\sin^2\alpha + htd_3^2\right), \quad H_{33} = E\left(\frac{th^3}{12}\cos^2\alpha + htd_2^2\right), \\ H_{23} &= E\left(\frac{th^3}{12}\sin\alpha\cos\alpha + htd_2d_3\right) = E\left(\frac{th^3}{24}\sin 2\alpha + htd_2d_3\right). \end{aligned} \tag{6.53}$$

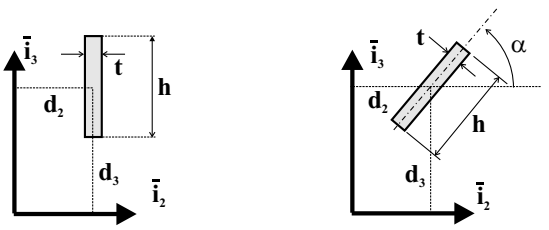

Fig. 6.13. A thin rectangular strip.

Example 6.3. Bending stiffness of a trapezoidal section - Approach 1
Consider the trapezoidal section shown on the left in fig. 6.14. Because axis $\bar{\imath}_2$ is an axis of symmetry of the section, the centroid of the section is located along axis, *i.e.*, $x_{3c} = 0$, and axis $\bar{\imath}_2$ is a principal centroidal axis of bending. Using eqs. (6.52) and (6.53), the centroidal bending stiffness about axis $\bar{\imath}_2$ becomes

$$H_{22}^c = E\left[\frac{t(2h_1)^3}{12} + \frac{t(2h_2)^3}{12} + 2\frac{t\ell^3}{12}\sin^2\alpha + 2t\ell(\frac{h_1+h_2}{2})^2\right], \tag{6.54}$$

where $\ell = [b^2 + (h_2 - h_1)^2]^{1/2}$ is the length of the upper and lower flanges. The first two terms represent the contribution of the two webs evaluated with the help of eq. (6.52), whereas the last two terms give the contribution of the flanges obtained from eq. (6.53). It is clear that $\sin\alpha = (h_2 - h_1)/\ell$, and after simplification, the bending stiffness becomes

$$H_{22}^c = \frac{2Et}{3}\left[h_1^3 + h_2^3 + \ell(h_1^2 + h_2^2 + h_1 h_2)\right]. \tag{6.55}$$

The bending stiffness about axis $\bar{\imath}_3$ can be evaluated in a similar fashion. Note that the location of the centroid, x_{2c}, must be calculated first, because this quantity is required to evaluated H_{33}^c.

Example 6.4. Bending stiffness of a trapezoidal section - Approach 2

The problem treated in the previous examples can also be approached using the triangle area equivalence method depicted in the right part of fig. 6.12. Specifically, each straight segment of the cross-section is represented by three lumped areas located at the ends and midpoint of each segment. Figure 6.14 shows the thin-walled trapezoidal section and its lumped equivalent. Using the lumped areas, it follows that a calculation of H_{22}^c will require areas $\mathcal{A}_1$, $\mathcal{A}_2$, $\mathcal{A}_3$, $\mathcal{A}_5$, $\mathcal{A}_6$, $\mathcal{A}_7$; areas $\mathcal{A}_4$ and $\mathcal{A}_8$ are at a vanishing distance from axis $\bar{\imath}_2$ and hence, do not appear in the computation of the bending stiffness H_{22}^c. The other areas are $\mathcal{A}_1 = \mathcal{A}_7 = 1/6\ (2h_2 t + \ell t)$, $\mathcal{A}_2 = \mathcal{A}_6 = 2/3\ \ell t$ and $\mathcal{A}_3 = \mathcal{A}_5 = 1/6\ (2h_1 t + \ell t)$, leading to

$$\begin{aligned} H_{22}^c &= 2E\left[\frac{1}{6}(2h_1 t + \ell t)h_1^2 + \frac{2}{3}\ell t(\frac{h_1 + h_2}{2})^2 + \frac{1}{6}(2h_2 t + \ell t)h_2^2\right], \\ &= \frac{Et}{3}\left[2h_1^3 + 2h_2^3 + \ell(h_1^2 + h_2^2) + \ell(h_1 + h_2)^2\right] \\ &= \frac{2Et}{3}\left[h_1^3 + h_2^3 + \ell(h_1^2 + h_2^2 + h_1 h_2)\right], \end{aligned}$$

which is identical to eq. (6.55).

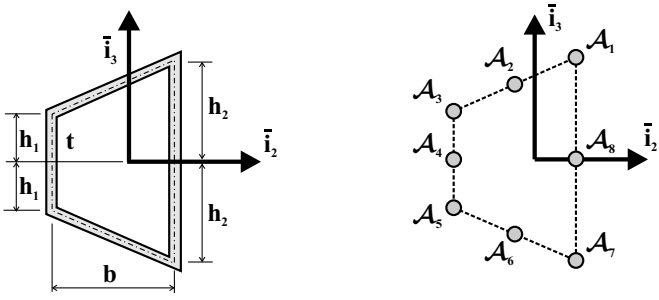

Fig. 6.14. Trapezoidal thin-walled section and lumped representation.

Example 6.5. Principal centroidal axes of an "L" shaped section
Consider the thin-walled, "L" shaped cross-section of a beam made of a homogeneous material of Young modulus E, as shown in fig. 6.15. Let $b = 0.25$ m , $h = 0.1$ m, and $t = 2.3$ mm. For convenience, a set of axes $(\bar{\imath}_2, \bar{\imath}_3)$ is defined, which is aligned with the flanges and has its origin at their intersection, point **A**; clearly, this axis system is not centroidal. The axial stiffness of the section is $S = Et(b + h)$ and the location of the centroid is then computed using eqs. (6.11), to find $x_{2c} = b^2/[2(b+h)]$ and $x_{3c} = h^2/[2(b + h)]$. A set of centroidal axes $(\bar{\imath}_2^c, \bar{\imath}_3^c)$ parallel to the flanges are shown in fig. 6.15.

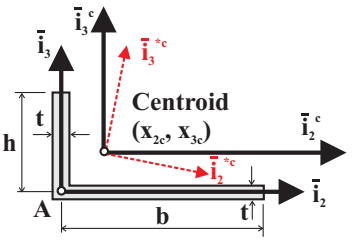

Fig. 6.15. Thin-walled, L shaped cross-section.

Next, the centroidal bending stiffnesses are computed with the help of the parallel axis theorem, eq. (6.45), as

$$H_{22}^c = E\left[\frac{th^3}{12} + ht\left(\frac{h}{2} - x_{3c}\right)^2 + bt\, x_{3c}^2\right] = \frac{Eth^3}{3}\left[1 - \frac{3h}{4(b+h)}\right],$$

and

$$H_{33}^c = E\left[\frac{tb^3}{12} + bt\left(\frac{b}{2} - x_{2c}\right)^2 + ht\, x_{2c}^2\right] = \frac{Etb^3}{3}\left[1 - \frac{3b}{4(b+h)}\right].$$

Although the centroidal axes $(\bar{\imath}_2^c, \bar{\imath}_3^c)$ are convenient to use because they are parallel to the flanges, *they are not principal axes*. Indeed, the cross bending stiffness, computed based on the parallel axis theorem, eq. (6.46), is

$$H_{23}^c = Eth\, x_{2c}\left[-\left(\frac{h}{2} - x_{3c}\right)\right] + Etb\left[-\left(\frac{b}{2} - x_{2c}\right)\right] x_{3c} = -\frac{Etb^2h^2}{4(b+h)}.$$

Using the numbers given above, the bending stiffnesses are evaluated as

$$\frac{H_{22}^c}{E} = 0.655 \times 10^{-6}\mathrm{m}^4,\ \frac{H_{33}^c}{E} = 6.04 \times 10^{-6}\mathrm{m}^4,\ \frac{H_{23}^c}{E} = -1.12 \times 10^{-6}\mathrm{m}^4.$$

The orientation of the principal centroidal axes then follows from eqs. (6.36)

$$\sin 2\alpha^* = \frac{H_{23}^c}{\Delta} = -0.3826; \quad \cos 2\alpha^* = \frac{H_{33}^c - H_{22}^c}{2\Delta} = 0.9239. \tag{6.56}$$

where $\Delta/E = \sqrt{(H^c_{33} - H^c_{22})^2/4 + (H^c_{23})^2} = 2.917 \times 10^{-6}$ m^4. Angle $2\alpha^*$ is in the fourth quadrant, and hence, $\alpha^* = -11.25$ deg. Finally, the principal centroidal bending stiffness are evaluated based on eq. (6.38) to find $H^{c*}_{22}/E = 432.8 \times 10^{-9}$ m^4 and $H^{c*}_{33}/E = 5.940 \times 10^{-6}$ m^4. The bending stiffness is minimum with respect to axis $\overline{\imath}^{*c}_2$ and maximum with respect to axis $\overline{\imath}^{*c}_3$.

6.8.5 Problems

Problem 6.1. Various questions on three-dimensional beam theory
(1) For a particular cross-section, the centroidal bending stiffnesses have been computed as H^c_{22}, H^c_{33}, and H^c_{23}. Next, the bending stiffnesses are computed about a set of parallel axes with their origin at an arbitrary point **D** and found to be H^d_{22}, H^d_{33}, and H^d_{23}. Is it possible to find a point **D** such that $H^d_{22} < H^c_{22}$? Why? *(2)* For a particular cross-section, the centroidal bending stiffnesses have been computed as H^c_{22}, H^c_{33}, and H^c_{23}. Next, the bending stiffnesses are computed about a set of parallel axes with their origin at an arbitrary point **D** and found to be H^d_{22}, H^d_{33}, and H^d_{23}. Is it possible to find a point **D** such that $H^d_{23} < H^c_{23}$? Why? *(3)* Consider a uniform cantilevered beam subjected to a uniform transverse loading distribution $p_0\bar{n}$, where $\bar{n}$ is a unit vector perpendicular to the axis of the beam, $\overline{\imath}_1$. Under what condition will the transverse deflection of the beam be oriented in the direction of $\bar{n}$? *(4)* For a particular cross-section, the principal centroidal bending stiffnesses have been computed as H^{c*}_{22} and H^{c*}_{33}, $H^{c*}_{22} \leq H^{c*}_{33}$. Next, the bending stiffnesses are computed about a set of non-principal axes, $\overline{\imath}_2$, $\overline{\imath}_3$ where axis $\overline{\imath}_2$ is at an arbitrary angle α with respect to $\overline{\imath}^*_2$, and found to be H^c_{22}, H^c_{33}, and H^c_{23}. Is it possible to find an angle α such that $H^c_{22} < H^{c*}_{22}$. Why? *(5)* A uniform cantilevered beam is subjected to a tip axial force. The beam is made of a homogeneous material. Under what condition will the strain distribution over the cross-section be uniform?

Problem 6.2. Axial stresses in a circular cross-section
Consider a solid circular section of radius R subjected to an axial force, N_1, and bending moments, M_2 and M_3. If the material has a yield strain ϵ_y, find the yield envelope for the section.

Problem 6.3. Three-dimensional bema theory
In section 5.6, the governing equations for a beam subjected to combined axial and transverse loads were developed. The origin of the axis system was located at an arbitrary point, *i.e.*, it was not coincident with the centroid of the cross-section. *(1)* Generalize the displacement field given by eq. (5.73) to accommodate general, three-dimensional deformations. *(2)* Find the corresponding strain field. *(3)* Develop the sectional constitutive laws. *(4)* Derive the equilibrium equations of the problem. *(5)* For the problem depicted in fig. 6.1, provide the governing equations and associated boundary conditions. *(6)* Clearly defined all the sectional stiffness coefficients appearing in your developments.

Problem 6.4. Principal axes of bending of a "Z" section
A beam made of a homogeneous material features the "Z" cross-section depicted in fig. 6.16. *(1)* Find the location of the centroid. *(2)* Find the bending stiffnesses in a coordinate system parallel to that shown on the figure, but with its origin at the centroid. *(3)* Find the orientation of the principal axes of bending. *(4)* Find the principal centroidal bending stiffnesses, H^{c*}_{22}, H^{c*}_{33}. Use $a/t = 10$.

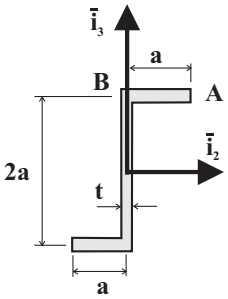

Fig. 6.16. "Z" shaped cross-section of a beam.

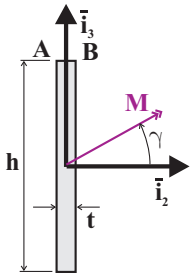

Fig. 6.17. Thin rectangular cross-section.

Problem 6.5. Neutral axis of a "Z" section
A beam made of a homogeneous material features the "Z" cross-section depicted in fig. 6.16. If a bending moment M_2 is applied to the section, find the equation of the neutral axis.

Problem 6.6. Stresses in a thin-walled rectangular cross-section
A beam made of a homogeneous material features the thin-walled rectangular cross-section depicted in fig. 6.17, with $h/t = 12$. A bending moment M is applied to the section and its axis is oriented at an angle γ with respect to axis $\bar{\imath}_2$. *(1)* Compute the axial stresses at points **A** and **B**. *(2)* On one graph, plot the non-dimensional stresses at points **A** and **B**, denoted $\sigma_1^{(A)}(\gamma)/\sigma_1^{(A)}(\gamma = 0)$ and $\sigma_1^{(B)}(\gamma)/\sigma_1^{(B)}(\gamma = 0)$, respectively, for $\gamma \in [0, \pi/2]$. *(3)* Let σ_y be the yield stress for the material. Plot the non-dimensional maximum bending moment the section can carry, $6M_{\max}/(th^2\sigma_y)$, as a function of $\gamma \in [-\pi/2, \pi/2]$. Comment on your results.

6.9 Summary of three-dimensional beam theory

Solving a three-dimensional beam problem involves determining the three components of displacement field of the beam, $\bar{u}_1(x_1)$, $\bar{u}_2(x_1)$, and $\bar{u}_3(x_1)$ and the axial stress distribution, $\sigma_1(x_1, x_2, x_3)$, over the cross-section.

A solution for the displacement field can be developed by following either of two equivalent approaches described below.

□ Deflection calculation: approach 1
1. Compute the location of the centroid using eq. (6.11).
2. Select a set of axes $\mathcal{I} = (\bar{\imath}_1, \bar{\imath}_2, \bar{\imath}_3)$, for which the $\bar{\imath}_1$ axis lies along the sectional centroids and project all applied loads along these axes.
3. Compute the sectional stiffness coefficients eqs. (6.5), (6.8), and (6.9).
4. Solve the axial problem (6.23a) and the two coupled bending differential equations (6.23b) to 6.23c, subjected to the boundary conditions (6.24) and (6.26).

□ Deflection calculation: approach 2
1. Compute the location of the centroid using eq. (6.11).

2. Compute the orientation of the principal centroidal axes of bending $\mathcal{I}^* = (\bar{\imath}_1^*, \bar{\imath}_2^*, \bar{\imath}_3^*)$, and the principal bending stiffnesses according to the procedure described in section 6.6.
3. Project all applied load along the principal centroidal axes of bending.
4. Solve the axial problem (6.30) and two uncoupled bending problems (6.31) and (6.32), subjected to the appropriate boundary conditions.

The two approaches will give identical results. The unknowns of the problem in the first approach are the displacement components $\bar{u}_1$, $\bar{u}_2$, and $\bar{u}_3$ along an arbitrary set of centroidal axes, whereas the displacement components $\bar{u}_1^*$, $\bar{u}_2^*$, and $\bar{u}_3^*$ along the principal centroidal axes of bending are the unknown of the second approach. The solution of the axial and two *coupled* differential equations of the first approach is, in general, quite difficult to obtain. In the second approach, additional work, namely the computation of the principal axes of bending orientation, is initially required. The solution phase then reduces to solving three *decoupled* differential equations.

Once the axial force and bending moment distributions are evaluated, the axial stress distribution is easily obtained. It is also possible to carry out the stress calculation using either the original centroidal axes or the principal centroidal axes of bending.

□ Axial stress calculation: approach 1
1. Compute the location of the centroid using eq. (6.11).
2. Select an axis system set of axes $\mathcal{I} = (\bar{\imath}_1, \bar{\imath}_2, \bar{\imath}_3)$, for which the $\bar{\imath}_1$ axis lies along the section centroids and project all applied loads along these axes.
3. Compute the sectional stiffness coefficients eqs. (6.5), (6.8), and (6.9).
4. Determine the bending moments, $M_2(x_1)$ and $M_3(x_1)$, at a particular axial location, x_1, and use either eq. (6.15) or (6.14) to compute the axial stress, σ_1 at any location on the cross-section.

□ Axial stress calculation: approach 2
1. Compute the location of the centroid using eq. (6.11).
2. Compute the orientation of the principal centroidal axes of bending $\mathcal{I}^* = (\bar{\imath}_1^*, \bar{\imath}_2^*, \bar{\imath}_3^*)$, and the principal bending stiffnesses according to the procedure described in section 6.6.
3. Project all applied load along the principal centroidal axes of bending.
4. Determine the bending moments, $M_2^*(x_1)$ and $M_3^*(x_1)$, at a particular axial location, x_1, and use eq. (6.29) to compute the axial stress, σ_1 at any location on the cross-section.

If the geometry of the cross-section is more easily expressed in axis system $\mathcal{I}$, approach 1will be more expeditious.

To demonstrate the use of these approaches for three-dimensional beams, a simple problem will be solved using both approaches, and the results will be shown to be identical.

Example 6.6. Bending of a Z section - Approach 1

Consider a thin-walled cantilevered beam subjected to a uniform transverse load, p_0, as depicted in fig. 6.18. The beam is clamped at the root and is unrestrained at the

tip. The beam is thin walled, *i.e.*, $t/a \ll 1$, and its "Z" shaped cross-section is made of a homogeneous material with a Young's modulus E. In approach 1, the solution will be developed in the axes aligned with the cross-section.

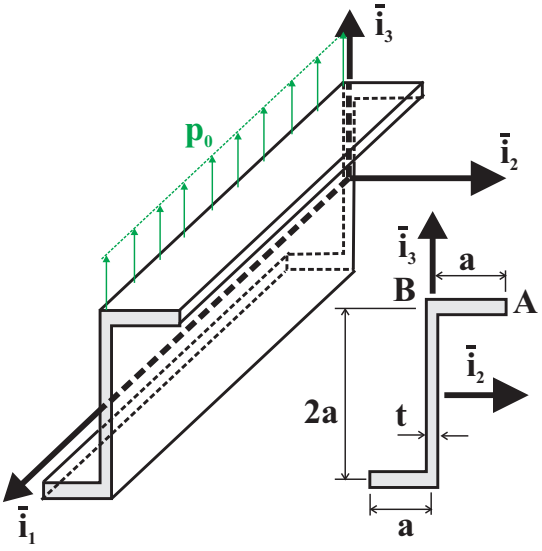

Fig. 6.18. Thin-walled cantilevered beam under a uniform transverse load.

Displacement calculations

A centroidal axis system is used with axis $\bar{\imath}_3$ aligned vertically as shown in fig. 6.18. This axis system makes it easy to locate different points on the cross-section. The first step is to compute the location of the centroid using eq. (6.11). Since the material is homogeneous, the location of the centroid is identical to that of the center of mass of the section and is located on the vertical web, midway between the upper and lower flanges. Axis system $\mathcal{I} = (\bar{\imath}_1, \bar{\imath}_2, \bar{\imath}_3)$ is located at the centroid, as shown in fig. 6.18. The next step is to compute the various sectional stiffnesses. The axial stiffness is computed first using eq. (6.5) to find $S = E\,[at + 2at + at] = 4atE$. The bending stiffnesses are computed from eq. (6.8)

$$H^c_{22} = E\left[\left(\frac{at^3}{12} + at\,a^2\right) + \frac{t(2a)^3}{12} + \left(\frac{at^3}{12} + at\,a^2\right)\right] \approx \frac{8a^3tE}{3};$$

$$H^c_{33} = E\left[\left(\frac{ta^3}{12} + at\,\frac{a^2}{4}\right) + \frac{2a(t)^3}{12} + \left(\frac{ta^3}{12} + at\,\frac{a^2}{4}\right)\right] \approx \frac{2a^3tE}{3},$$

where the thin wall approximation, $t/a \ll 1$, is used to simplify the results. Finally, the cross bending stiffness is obtained from eq. (6.9),

$$H_{23}^c = E\left[at\left(-\frac{a}{2}\right)(-a) + 2at(0)(0) + at\left(\frac{a}{2}\right)(a)\right] = a^3tE.$$

Although the selected centroidal axis system conveniently describes the geometry of the problem, it does not coincide with the principal axes of bending, which are characterized by a vanishing cross bending stiffness.

The fourth step of this approach is the solution of the governing equations. The axial and two bending governing equations can be written as

$$S\frac{\mathrm{d}^2\bar{u}_1}{\mathrm{d}x_1^2} = 0, \quad H_{33}^c\frac{\mathrm{d}^4\bar{u}_2}{\mathrm{d}x_1^4} + H_{23}^c\frac{\mathrm{d}^4\bar{u}_3}{\mathrm{d}x_1^4} = 0, \quad H_{23}^c\frac{\mathrm{d}^4\bar{u}_2}{\mathrm{d}x_1^4} + H_{22}^c\frac{\mathrm{d}^4\bar{u}_3}{\mathrm{d}x_1^4} = p_0.$$

The boundary conditions at the root are purely geometric and are given by eqs. (6.24), which specify that the axial displacement and the transverse displacements and slopes must all vanish.

The boundary conditions at the tip are a bit more complicated. Since no axial force is applied, the axial boundary condition at the tip requires $N_1 = 0$ or $N_1 = S\mathrm{d}\bar{u}_1/\mathrm{d}x_1 = 0$, which implies $\mathrm{d}\bar{u}_1/\mathrm{d}x_1 = 0$ at $x_1 = L$. Similarly, at the tip of the beam, the two bending moments must vanish, $M_2(L) = M_3(L) = 0$, and hence

$$\left[H_{23}^c\frac{\mathrm{d}^2\bar{u}_2}{\mathrm{d}x_1^2} + H_{22}^c\frac{\mathrm{d}^2\bar{u}_3}{\mathrm{d}x_1^2}\right]_{x_1=L} = \left[H_{33}^c\frac{\mathrm{d}^2\bar{u}_2}{\mathrm{d}x_1^2} + H_{23}^c\frac{\mathrm{d}^2\bar{u}_3}{\mathrm{d}x_1^2}\right]_{x_1=L} = 0.$$

Finally, the shear forces must also vanish at the beam's tip, $V_2(L) = V_3(L) = 0$, leading to

$$\left[-H_{33}^c\frac{\mathrm{d}^3\bar{u}_2}{\mathrm{d}x_1^3} - H_{23}^c\frac{\mathrm{d}^3\bar{u}_3}{\mathrm{d}x_1^3}\right]_{x_1=L} = \left[H_{23}^c\frac{\mathrm{d}^3\bar{u}_2}{\mathrm{d}x_1^3} + H_{22}^c\frac{\mathrm{d}^3\bar{u}_3}{\mathrm{d}x_1^3}\right]_{x_1=L} = 0.$$

The axial equation is decoupled from the two bending equations. Its solution for homogeneous boundary conditions is the trivial solution, $\bar{u}_1 = 0$, which means that there is no axial displacement of the beam's centroid.

The two bending equations are coupled, but a simple algebraic manipulation yields two uncoupled equations for this problem

$$\begin{aligned}\frac{\mathrm{d}^4\bar{u}_2}{\mathrm{d}x_1^4} &= -\frac{H_{23}^c p_0}{H_{22}^c H_{33}^c - H_{23}^c H_{23}^c} = -\frac{9p_0}{7a^3tE},\\ \frac{\mathrm{d}^4\bar{u}_3}{\mathrm{d}x_1^4} &= \frac{H_{33}^c p_0}{H_{22}^c H_{33}^c - H_{23}^c H_{23}^c} = \frac{6p_0}{7a^3tE}.\end{aligned}$$

The boundary conditions can be decoupled in a similar manner to yield $\bar{u}_2 = \mathrm{d}\bar{u}_2/\mathrm{d}x_1 = 0$ and $\bar{u}_3 = \mathrm{d}\bar{u}_3/\mathrm{d}x_1 = 0$, at $x_1 = 0$ and $\mathrm{d}\bar{u}_2^2/\mathrm{d}x_1^2 = \mathrm{d}\bar{u}_2^3/\mathrm{d}x_1^3 = 0$ and $\mathrm{d}\bar{u}_3^2/\mathrm{d}x_1^2 = \mathrm{d}\bar{u}_3^3/\mathrm{d}x_1^3 = 0$ at $x_1 = L$. Solving these two decoupled, fourth order differential equations gives the solution of the problem

$$\bar{u}_2(x_1) = -\frac{3p_0L^4}{56a^3tE}\left(\eta^4 - 4\eta^3 + 6\eta^2\right), \tag{6.57}$$

$$\bar{u}_3(x_1) = \frac{p_0 L^4}{28 a^3 t E}\left(\eta^4 - 4\eta^3 + 6\eta^2\right), \tag{6.58}$$

where $\eta = x_1/L$ is the non-dimensional variable along the beam's span. The displacements at the tip of the beam are $\bar{u}_2^{\text{tip}} = -9/56\ p_0 L^4/(a^3 t E)$ and $\bar{u}_3^{\text{tip}} = 6/56\ p_0 L^4/(a^3 t E)$.

Bending stress calculation

The axial stress due to bending, σ_1, can be computed from eqs. (6.14) or (6.15), but eq. (6.14) is preferable because the coordinates of a point on the section, (x_2, x_3), explicitly appear in this equation. For this problem, the stress resultants are obtained from equilibrium considerations as $M_2 = p_0 L^2(1-\eta)^2/2$, $N_1 = 0$ and $M_3 = 0$, and hence,

$$\begin{aligned}
\sigma_1(\eta, x_2, x_3) =& \frac{E}{H_{22}^c H_{33}^c - H_{23}^c H_{23}^c}\left[-x_2 H_{23}^c M_2(\eta) + x_3 H_{33}^c M_2(\eta)\right] \\
=& \frac{9E}{7(a^3 t E)^2}\left[-x_2(a^3 t E) + x_3\left(\frac{2}{3}a^3 t E\right)\right] M_2(\eta) \\
=& \frac{3}{7a^3 t}(-3x_2 + 2x_3)\frac{p_0 L^2}{2}(1-\eta)^2.
\end{aligned}$$

A number of conclusions can be drawn from this result.

1. Axial stresses vary along the span of the beam because they depend on η. Stresses are maximum where $M_2(\eta)$ is a maximum, *i.e.*, at the root of the beam.
2. For this loading case, it is possible to define the neutral axis of the section. Setting $\sigma_1 = 0$, yields the equation for the neutral axis: $-3x_2 + 2x_3 = 0$. The neutral axis is a line in the plane of the cross-section that makes a 56° angle with axis $\bar{\imath}_2$. Axial stresses are positive on one side of this axis and negative on the other.
3. Axial stresses vary over the cross-section of the beam, *i.e.*, they depend on x_2 and x_3. At any given span-wise location, extremum axial stresses are found in non-dimensional form at points **A** ($x_2 = a, x_3 = a$) or **B** ($x_2 = 0, x_3 = a$), see fig. 6.18:

$$\frac{\sigma_1^{(A)} a^2 t}{M_2(x_1)} = -\frac{3}{7}, \quad \frac{\sigma_1^{(B)} a^2 t}{M_2(x_1)} = \frac{6}{7}.$$

The maximum magnitude is found at point **B**.

Example 6.7. Bending of a Z section - approach 2

In this example, the same problem treated in the previous example will be solved in the principal axes.

Displacement calculation

The first step of this second approach is once again the computation of the location of the centroid using eq. (6.11); it is located on the web, midway between the flanges. The next step is computation of the orientation of the principal centroidal axes of bending. Equation (6.36) yields

$$\sin 2\alpha^* = \frac{a^3 tE}{a^3 tE\sqrt{2}} = \frac{1}{\sqrt{2}}, \quad \cos 2\alpha^* = -\frac{a^3 tE}{a^3 tE\sqrt{2}} = -\frac{1}{\sqrt{2}}.$$

Thus, the principal axis of bending $\bar{\imath}_2^*$ is oriented at an angle $\alpha^* = 67.5^\circ$ with respect to axis $\bar{\imath}_2$, as shown in fig. 6.19. The principal centroidal bending stiffnesses are found from eq. (6.38)

$$H_{22}^{c*} = \frac{5a^3 tE}{3} - a^3 tE\sqrt{2} = \left(\frac{5}{3} - \sqrt{2}\right) a^3 tE, \quad H_{33}^{c*} = \left(\frac{5}{3} + \sqrt{2}\right) a^3 tE.$$

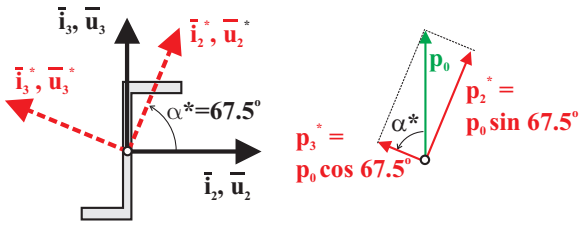

Fig. 6.19. The principal axes of bending for the thin walled section.

The applied load is now projected along the directions of the principal axes of bending to find

$$p_2^* = p_0 \sin 67.5^\circ, \quad p_3^* = p_0 \cos 67.5^\circ.$$

The last step consists of the solution of three independent problems. As in the first approach, the extensional problem yields $\bar{u}_1^* = 0$. The two decoupled bending problems are

$$H_{33}^{c*} \frac{\mathrm{d}^4 \bar{u}_2^*}{\mathrm{d}x_1^{*4}} = p_0 \sin 67.5^\circ, \quad H_{22}^{c*} \frac{\mathrm{d}^4 \bar{u}_3^*}{\mathrm{d}x_1^{*4}} = p_0 \cos 67.5^\circ.$$

subjected to the following boundary conditions at the root $\bar{u}_2^* = \mathrm{d}\bar{u}_2^*/\mathrm{d}x_1^* = 0$, $\bar{u}_3^* = \mathrm{d}\bar{u}_3^*/\mathrm{d}x_1^* = 0$ and at the tip $\mathrm{d}^2\bar{u}_2^*/\mathrm{d}x_1^{*2} = \mathrm{d}^3\bar{u}_2^*/\mathrm{d}x_1^{*3} = 0$, $\mathrm{d}^2\bar{u}_3^*/\mathrm{d}x_1^{*2} = \mathrm{d}^3\bar{u}_3^*/\mathrm{d}x_1^{*3} = 0$. The solution of these two decoupled equations is:

$$\bar{u}_2^*(\eta) = \frac{p_0 \sin 67.5^\circ}{H_{33}^{c*}} \frac{L^4}{24} \left(\eta^4 - 4\eta^3 + 6\eta^2\right), \tag{6.59}$$

$$\bar{u}_3^*(\eta) = \frac{p_0 \cos 67.5^\circ}{H_{22}^{c*}} \frac{L^4}{24} \left(\eta^4 - 4\eta^3 + 6\eta^2\right). \tag{6.60}$$

The corresponding non-dimensional deflections at the tip of the beam become

$$\frac{\bar{u}^*_{2\text{tip}}a^3tE}{p_0L^4} = \frac{\sin 67.5^\circ}{8(5/3+\sqrt{2})} = 0.0375, \quad \frac{\bar{u}^*_{3\text{tip}}a^3tE}{p_0L^4} = \frac{\cos 67.5^\circ}{8(5/3-\sqrt{2})} = 0.1895.$$

To compare the results obtained with approaches 1 and 2, their respective predictions must be expressed in the same axis system. Displacement components $\bar{u}_2$ and $\bar{u}_3$ obtained with approach 1 and given by eqs. (6.57) and (6.58), respectively, are the displacement components of along axes $\bar{\imath}_2$ and $\bar{\imath}_3$, respectively, whereas the displacements components $\bar{u}^*_2$ and $\bar{u}^*_3$ obtained with approach 2 and given by eqs. (6.59) and (6.60), respectively, are the displacement components along the principal centroidal axes of bending $\bar{\imath}^*_2$ and $\bar{\imath}^*_3$, respectively. These two results describe identical displacements of the beam. Indeed, fig. 6.19 shows that the two sets of displacement are related through the following transformations: $\bar{u}^*_2 = \bar{u}_2\cos 67.5^\circ + \bar{u}_3\sin 67.5^\circ$ and $\bar{u}^*_3 = -\bar{u}_2\sin 67.5^\circ + \bar{u}_3\cos 67.5^\circ$. Using these equations to compute the non-dimensional tip displacements yields

$$\frac{\bar{u}^*_{2\text{tip}}a^3tE}{p_0L^4} = \left(-\frac{9}{56}\cos 67.5^\circ + \frac{3}{28}\sin 67.5^\circ\right) = 0.0375,$$

$$\frac{\bar{u}^*_{3\text{tip}}a^3tE}{p_0L^4} = \left(\frac{9}{56}\sin 67.5^\circ + \frac{3}{28}\cos 67.5^\circ\right) = 0.1895,$$

which agree exactly with the above results.

Bending stress calculation

The axial stress due to bending, σ^*_1, is now computed using eq. (6.29) where $N^*_1 = 0$. The bending moment components, M^*_2 and M^*_3, about axes $\bar{\imath}^*_2$ an $\bar{\imath}^*_2$, respectively, are related to their counterparts, M_2 and M_3, about axes $\bar{\imath}_2$ and $\bar{\imath}_3$, respectively, as $M^*_2(\eta) = M_2(\eta)\cos 67.5^\circ$ and $M^*_3(\eta) = -M_2(\eta)\sin 67.5^\circ$. The axial stress distribution becomes

$$\frac{\sigma^*_1 at^3}{M_2} = x^*_3\frac{\cos 67.5^\circ}{(5/3-\sqrt{2})} + x^*_2\frac{\sin 67.5^\circ}{(5/3+\sqrt{2})}.$$

To reconcile these results with those obtained with approach 1, it is necessary to perform a coordinate transformation between the coordinate x^*_2 and x^*_3 of a point on the cross-section expressed in the principal centroidal axes of bending, $\mathcal{I}^* = (\bar{\imath}^*_2, \bar{\imath}^*_3)$, to the counterparts in coordinate system $\mathcal{I} = (\bar{\imath}_2, \bar{\imath}_3)$: $x^*_2 = x_2\cos 67.5^\circ + x_3\sin 67.5^\circ$ and $x^*_3 = -x_2\sin 67.5^\circ + x_3\cos 67.5^\circ$.

For instance, at point **A**, $x_2 = a, x_3 = a$, and the axial stress becomes

$$\frac{\sigma^{*A}_1 a^2 t}{M_2(\eta)} = \left[\frac{(\cos 67.5^\circ + \sin 67.5^\circ)\sin 67.5^\circ}{5/3+\sqrt{2}} + \frac{(-\sin 67.5^\circ + \cos 67.5^\circ)\cos 67.5^\circ}{5/3-\sqrt{2}}\right] = -0.43.$$

Similarly, at point **B**, $x_2 = 0, x_3 = a$, and the axial stress follows as

$$\frac{\sigma_1^{*B} a^2 t}{M_2} = \frac{\sin^2 67.5^\circ}{5/3 + \sqrt{2}} + \frac{\cos^2 67.5^\circ}{5/3 - \sqrt{2}} = 0.86.$$

As expected, these results are identical to those obtained using approach 1.

6.9.1 Discussion of the results

Although the applied load acts in the $\bar{\imath}_3$ direction only, the beam displaces along *both axes* $\bar{\imath}_3$ *and* $\bar{\imath}_2$. In fact, the tip displacement component along axis $\bar{\imath}_2$ is *larger* than that along axis $\bar{\imath}_3$. This is due to the fact that bending in planes $(\bar{\imath}_1, \bar{\imath}_2)$ and $(\bar{\imath}_1, \bar{\imath}_3)$ is coupled, as expressed by the coupled governing equations (6.23a), (6.23b), and (6.23c).

This behavior is more easily understood when considering the results of the second approach expressed in the principal centroidal axes of bending. Indeed, the bending behavior of the beam along the principal axes of bending is *decoupled*. This means that load p_2^*, applied along axis $\bar{\imath}_2^*$, produces a displacement *along axis* $\bar{\imath}_2^*$ *only*. Similarly, load p_3^*, applied along axis $\bar{\imath}_3^*$, produces a displacement *along axis* $\bar{\imath}_3^*$ *only*. The displacement along axis $\bar{\imath}_2^*$ is fairly small because the bending stiffness, H_{33}^{c*}, that characterizes bending about axis $\bar{\imath}_3^*$ is maximum. On the other hand, the displacement along axis $\bar{\imath}_3^*$ is large because the bending stiffness, H_{22}^{c*}, that characterizes bending about axis $\bar{\imath}_2^*$ is minimum. The resulting displacement, $\bar{u}_3^*$, when resolved along the axes $\bar{\imath}_2$ and $\bar{\imath}_3$, has the expected upward component, together with a *leftward* component. This explains the negative sign of the $\bar{u}_2$ in eq. (6.57).

6.10 Problems

Problem 6.7. Sectional bending stiffness
Consider the solid cross-section depicted in fig. 6.20. *(1)* Determine the location of the centroidal of the section. *(2)* Compute the sectional centroidal bending stiffnesses. *(3)* Determine the orientation of the principal centroidal axes of bending. *(4)* Compute the principal centroidal bending stiffnesses.

Problem 6.8. Beam with and "L" shaped cross-section
The "L" shaped cross-section beam shown in fig. 6.21 is subjected to a bending moment of magnitude M_b, which is acting in the direction indicated in the figure. Create and use a spreadsheet to accomplish the following tasks. Make your spreadsheet general so that different dimensions can be entered into the spreadsheet along with different values for the load and its orientation. The spreadsheet outputs should be in clearly labeled cells. *(1)* Determine the centroid location. *(2)* Determine the axial and bending stiffnesses in the centroidal axis system $\mathcal{I}^c = (\bar{\imath}_2^c, \bar{\imath}_3^c)$ indicated on the figure. *(3)* Using this axis system, compute the orientation of the neutral axis and compute magnitude and location of the maximum axial stress, $|\sigma_1^{\max}|$. *(4)* Find the orientation of the principal centroidal axes of bending, $\mathcal{I}^{c*} = (\bar{\imath}_2^{c*}, \bar{\imath}_3^{c*})$. *(5)* Using these axes, determine the magnitude and location of the maximum axial stress. Verify that this is the same result as in step *3*. Use the following data: $h = 150$ mm, $b = 100$ mm, $t_h = 10$ mm, $t_b = 14$ mm, $\theta = 30$ degrees, and $M_b = 10$ kN·m.

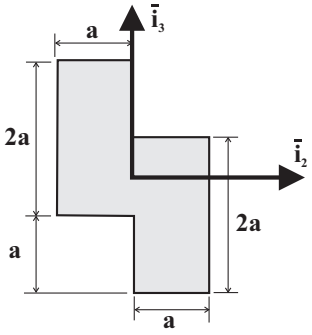

Fig. 6.20. Double-rectangular section.

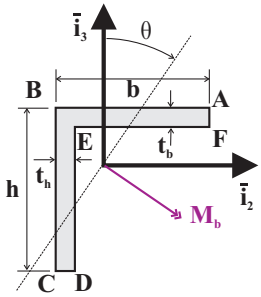

Fig. 6.21. "L" shaped cross-section.

Problem 6.9. Beam with "C" shaped cross-section

The "C" shaped cross-section beam shown in fig. 6.22 is subjected to a bending moment of magnitude M_b, which is acting in the direction indicated in the figure. Create and use a spreadsheet to accomplish the following tasks. Make your spreadsheet general so that different dimensions can be entered into the spreadsheet along with different values for the load and its orientation. The spreadsheet outputs should be in clearly labeled cells. *(1)* Determine the centroid location. *(2)* Determine the axial and bending stiffnesses in the centroidal axis system $\mathcal{I}^c = (\bar{\imath}_2^c, \bar{\imath}_3^c)$ indicated on the figure. *(3)* Using this axis system, compute the orientation of the neutral axis and compute magnitude and location of the maximum axial stress, $|\sigma_1^{\max}|$. *(4)* Find the orientation of the principal centroidal axes of bending, $\mathcal{I}^{c*} = (\bar{\imath}_2^{c*}, \bar{\imath}_3^{c*})$. *(5)* Using these axes, determine the magnitude and location of the maximum axial stress. Verify that this is the same result as in step *3*. Use the following data: $t_a = 15$ mm, $t_b = 30$ mm, $b_a = 30$ mm, $b_b = 40$ mm, $t_w = 20$ mm, and $h = 100$ mm, $\theta = -45$ degrees, and $M_b = 20$ kN·m.

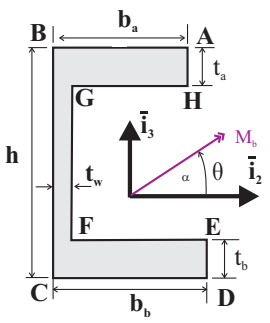

Fig. 6.22. "C" shaped cross-section.

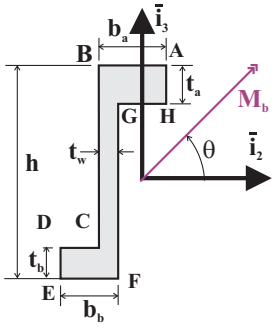

Fig. 6.23. "Z" shaped cross-section.

Problem 6.10. Beam with "Z" section

The "Z" shaped cross-section beam shown in fig. 6.23 is subjected to a bending moment of magnitude M_b, which is acting in the direction indicated in the figure. Create and use a spreadsheet to accomplish the following tasks. Make your spreadsheet general so that different dimensions can be entered into the spreadsheet along with different values for the load and

its orientation. The spreadsheet outputs should be in clearly labeled cells. *(1)* Determine the centroid location. *(2)* Determine the axial and bending stiffnesses in the centroidal axis system $\mathcal{I}^c = (\bar{\imath}_2^c, \bar{\imath}_3^c)$ indicated on the figure. *(3)* Using this axis system, compute the orientation of the neutral axis and compute magnitude and location of the maximum axial stress, $|\sigma_1^{\max}|$. *(4)* Find the orientation of the principal centroidal axes of bending, $\mathcal{I}^{c*} = (\bar{\imath}_2^{c*}, \bar{\imath}_3^{c*})$. *(5)* Using these axes, determine the magnitude and location of the maximum axial stress. Verify that this is the same result as in step *3*. Use the following data: $h = 95$ mm, $b_a = 30$ mm, $b_b = 50$ mm, $t_w = 20$ mm, $t_a = 15$ mm, and $t_b = 30$ mm, $\theta = -45$ degrees, and $M_b = 10$ kN·m.

Problem 6.11. Thin-walled "L" section

Consider the thin-walled, "L" shaped cross-section of a beam as shown in fig. 6.15. Let $b = 0.25$ m , $h = 0.1$ m, and $t = 2.5$ mm. *(1)* Find the location of the centroid of the section. *(2)* Find the orientation of the principal centroidal axes of bending.

Problem 6.12. Beam with "T" shaped cross-section

The "T" shaped cross-section beam shown in fig. 6.24 is subjected to a bending moment of magnitude M_b, which is acting in the direction indicated in the figure. Create and use a spreadsheet to accomplish the following tasks. Make your spreadsheet general so that different dimensions can be entered into the spreadsheet along with different values for the load and its orientation. The spreadsheet outputs should be in clearly labeled cells. *(1)* Determine the centroid location. *(2)* Determine the axial and bending stiffnesses in the centroidal axis system $\mathcal{I}^c = (\bar{\imath}_2^c, \bar{\imath}_3^c)$ indicated on the figure. *(3)* Using this axis system, compute the orientation of the neutral axis and compute magnitude and location of the maximum axial stress, $|\sigma_1^{\max}|$. *(4)* Find the orientation of the principal centroidal axes of bending, $\mathcal{I}^{c*} = (\bar{\imath}_2^{c*}, \bar{\imath}_3^{c*})$. *(5)* Using these axes, determine the magnitude and location of the maximum axial stress. Verify that this is the same result as in step *3*. Use the following data: $h = 140$ mm, $b = 120$ mm, $t_h = 12$ mm, $t_b = 10$ mm, and $a = 15$ mm, $\theta = -45$ degrees, and $M_b = 10$ kN·m.

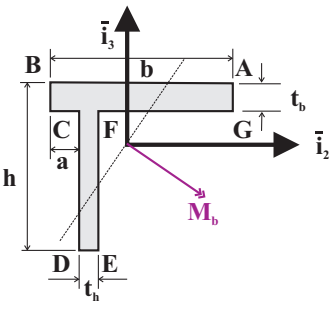

Fig. 6.24. "T" shaped cross-section.

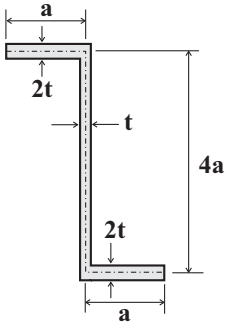

Fig. 6.25. Reversed "Z" shaped cross-section.

Problem 6.13. Thin-walled "Z" section

A beam is made of a homogeneous material of Young's modulus, E, and has the unsymmetric, thin-walled cross-section shown in fig 6.25. *(1)* Compute the centroidal stiffnesses in the coordinate system indicated on the figure. *(2)* Compute the orientation of the neutral axis for

the loading case where $M_2 \neq 0$, $M_3 = 0$. *(3)* Using the orientation of the neutral axis, determine the points on the section where the bending stress will have the maximum positive and negative values.

Problem 6.14. Thin-walled inverted "V" section

A thin-walled beam of length L and with cross-section shown in fig. 6.26 is simply supported at both ends and carries a distributed loading, p_0, acting upwards. *(1)* Find the maximum direct stress due to bending and where it acts. *(2)* Sketch the distribution of axial stress on the cross-section of the beam where the maximum bending stress acts.

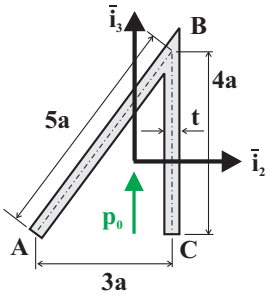

Fig. 6.26. Inverted "V" shaped cross-section.

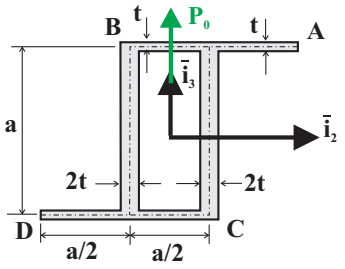

Fig. 6.27. Box$Z$ shaped cross-section.

Problem 6.15. Thin-walled cantilever beam with Box-Z section

A thin-walled cantilevered beam of length L and elastic modulus E is constructed with a cross-section shown in fig. 6.27. A vertical load P is applied at the tip of the beam. *(1)* Determine the axial stress acting at the root of the cantilever at point **A** and **B**. *(2)* Determine the deflection of the tip using the given centroidal axes. *(3)* Determine the tip deflection using the principal axes of bending, and show that they are equivalent to the results obtained in *(2)*. Hint: this is a numerically tedious problem, and use of a spreadsheet or computer program can be very effective.

Problem 6.16. Cantilevered beam with a "T" shaped cross-section

Consider the cantilevered beam of length L with a thin-walled "T" cross-section as depicted in fig. 6.28. A tip axial load P acts at the left edge of the top flange. A transverse tip load R acts in the plane of the tip cross-section in the direction indicated on the figure. *(1)* Find the principal centroidal axes of bending, $\bar{\imath}_1^*$, $\bar{\imath}_2^*$ and $\bar{\imath}_3^*$, of the cross-section. *(2)* Write the three uncoupled equations governing this problem and the corresponding boundary conditions. *(3)* Compute all the stiffness constants appearing in the equations, but do not solve the problem.

Problem 6.17. Cantilevered beam with "Z" shaped cross-section

Figure 6.29 depicts a cantilevered beam with a thin-walled "Z" shaped cross-section subjected to an axial load P applied at point **A** located at the lower left corner of the cross-section. *(1)* Determine the location of centroid of the section and locate the axis system at this point (with axis $\bar{\imath}_3$ parallel to the web). *(2)* Determine the bending stiffnesses H_{22}^c, H_{33}^c, and H_{23}^c for the centroidal axis system. *(3)* Determine the orientation of the principal axes of bending, $\bar{\imath}_2^*$ and $\bar{\imath}_3^*$, and the principal centroidal bending stiffnesses H_{22}^{c*}, H_{33}^{c*}. *(4)* Solve this problem in the centroidal coordinate system to determine the lateral displacements of the cross-section,

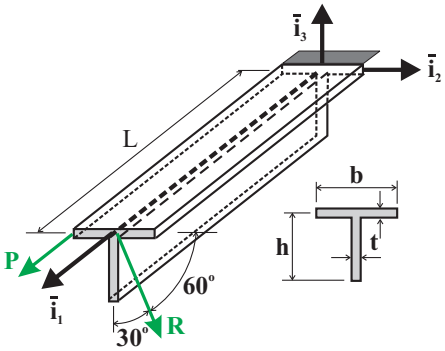

Fig. 6.28. Cantilevered beam with "T" shaped section under tip axial loads.

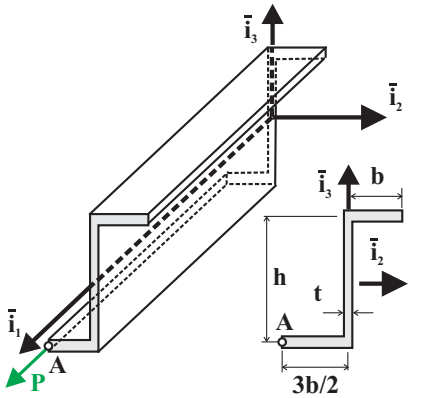

Fig. 6.29. Cantilevered beam with "Z" shaped section under tip axial load.

$\bar{u}_2(x_1)$ and $\bar{u}_3(x_1)$. *(5)* Solve this problem in the coordinate system defined by the principal axes of bending to determine the lateral displacements, $\bar{u}_2^*(x_1)$ and $\bar{u}_3^*(x_1)$. *(6)* Show that the two above solutions are identical. *(7)* Find the two components of displacement at the point of application of the load P which can be in non-dimensional terms as $Eb\bar{u}_2/P$ and $Eb\bar{u}_3/P$, respectively. *(8)* Find the axial stress distribution at the root of the beam. Plot this distribution along the web and flanges. Where does the maximum axial stress occur? Express this as a non-dimensional stress $b^2\sigma_1/P$. Use the following data: $L = 10b$, $h = 2b$ and $t = b/10$.

Problem 6.18. Cantilevered beam with a "U" shaped cross-section

Consider the cantilevered beam of length L with a thin-walled "U" shaped cross-section as depicted in fig. 6.30. A tip axial load, P, acts at the lower right corner of the section. Two transverse tip loads, both of magnitude R, act down in the plane of the tip cross-section. *(1)* Find the principal centroidal axes of bending, $\bar{i}_1^*$, $\bar{i}_2^*$ and $\bar{i}_3^*$, of the cross-section. *(2)* Write the three uncoupled equations governing this problem and the corresponding boundary conditions. *(3)* Compute all the stiffness constants appearing in the equations, but do not solve the problem.

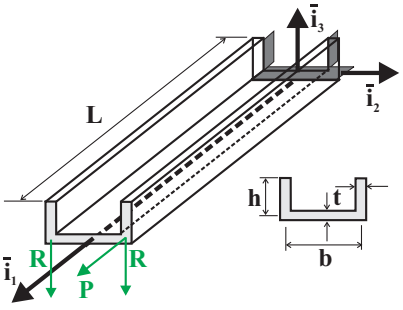

Fig. 6.30. Cantilevered beam with "U" shaped section under tip axial loads.